Zhang J, Fukuhara S, Sako K, Takenouchi T, Kitani H, Kume T, Koh GY, Mochizuki N.	Angiopoietin-1/Tie2 Signal Augments Basal Notch Signal Controlling Vascular Quiescence by Inducing Delta-Like 4 Expression through AKT-mediated Activation of {beta}-Catenin.	J. Biol. Chem	286	8055-8066	2011
Wakayama Y, Miura K, Hisataka S, Mochizuki N.	EphrinA1-EphA2 signal induces compaction and polarization of MDCK cells by inactivating ezrin through negative regulation of RhoA.	J. Biol. Chem	286	44243-53	2011
Minami M, Koyama T, Wakayama Y, Fukuhara S, Mochizuki N.	EphrinA/EphA signal facilitates insulin-like growth factor-I-induced myogenic differentiation through suppression of the Ras/extracellular signal-regulated kinase 1/2 cascade in myoblast cell lines.	Mol. Biol. Cell	22	3508-3519	2011
Watanabe T, Okada Y, Hoshikawa Y, Eba S, Notsuda H, Watanabe Y, Ohishi H, Sato Y, Kondo T	A Potent Anti-angiogenic Factor, Vasohibin-1, Ameliorates Experimental Bronchiolitis Obliterans.	Transplant Proc.	44	1155-1157	2012
Miyazaki Y, Kosaka T, Mikami S, Kikuchi E, Tanaka N, Maeda T, Ishida M, Miyajima A, Nakagawa K, Okada Y, Sato Y, Oya M	The prognostic significance of vasohibin-1 expression in patients with upper urinary tract urothelial carcinoma.	Clin Cancer Res.	18	4145-4153	2012
Takahashi Y, Koyanagi T, Suzuki Y, Saga Y, Kanomata N, Moriya T, Suzuki M, Sato Y	Vasohibin-2 expressed in human serous ovarian adenocarcinoma accelerates tumor growth by promoting angiogenesis.	Mol. Cancer Res.	10	1135-1146	2012
Miyashita H, Watanabe T, Hayashi H, Suzuki Y, Nakamura T, Ito S, Ono M, Hoshikawa Y, Okada Y, Kondo T, Sato Y	Angiogenesis inhibitor vasohibin-1 enhances stress resistance of endothelial cells via induction of SOD2 and SIRT1.	PLoS One	7	E46459	2012

Sato Y.	The Vasohibin Family: Novel Regulators of Angiogenesis.	Vascular Pharmacology	56	262-266	2012
Kajiya K. et al	Promotion of Lymphatic Integrity by Angiopoietin-1/Tie2 Signaling during Inflammation.	Am J Pathol	180	1273-1282	2012
Takakura N.	Guest editorial: mutual relationship between vascular biology and hematology.	Int J Hematol	95	117-118	2012
Takakura N.	Involvement of non-vascular stem cells in blood vessel formation.	Int J Hematol	95	138-142	2012
Takakura N.	Formation and regulation of the cancer stem cell niche.	Cancer Sci	103	1177-1181	2012
Kinugasa Y et al	Monoclonal Antibody Selectively Recognizing Murine But Not Human CD44.	Hybridoma	31	262-266	2012
Kidoya H et al	Biology of the apelin-APJ axis in vascular formation.	J Biochem	152	125-131	2012
Sakimoto S et al	A role for endothelial cells in promoting the maturation of astrocytes through the apelin/APJ system in mice.	Development	139	1327-1335	2012
Kidoya H et al	The apelin/APJ system induces maturation of the tumor vasculature and improves the efficiency of immune therapy.	Oncogene	31	3254-3264	2012
Yoshioka K et al	Endothelial PI3K-C2α, a class II PI3K, has an essential role in angiogenesis and vascular barrier function.	Nat Med	18	1560-1569	2012
Komada Y et al	Origins and properties of dental, thymic, and bone marrow mesenchymal cells and their stem cells.	PLoS One	7	e46436	2012
Maruyama K et al	The Transcription Factor Jdp2 Controls Bone Homeostasis and Antibacterial Immunity by Regulating Osteoclast and Neutrophil Differentiation	Immunity	37	1024-1036	2012

Muramatsu F et al	microRNA-125b inhibits tube formation of blood vessels through translational suppression of VE-cadherin.	Oncogene	32	414-421	2012
Satoh T et al	Critical role of Trib1 in differentiation of tissue-resident M2-like macrophages.	Nature	495	524-528	2012
Takeuchi S et al	Dual inhibition of Met kinase and angiogenesis to overcome HGF-induced EGFR-TKI resistance in *EGFR* mutant lung cancer.	Am J Pathol	181	1034-43	2012
Yamada T et al	Paracrine receptor activation by microenvironment triggers bypass survival signals and ALK inhibitor-resistance in EML4-ALK lung cancer cells.	Clin Cancer Res	18	3592-602	2012
Nakagawa T et al	Combined therapy with mutant-selective EGFR inhibitor and Met kinase inhibitor to overcome erlotinib resistance in *EGFR* mutant lung cancer.	Mol Cancer Ther	11	2149-2157	2012
Ohtsubo K et al	Endoscopic findings of upper gastrointestinal lesions in patients with pancreatic cancer.	JOP	13	420-426	2012
Kurai J et al	Therapeutic antitumor efficacy of anti-epidermal growth factor receptor antibody, cetuximab, against malignant pleural mesothelioma.	Int J Oncol	41	1610-1618	2012
Uramoto H et al	Prognostic value of aquired resistance-related molecules in Japanese patients with NSCLC treated with an EGFR-TKI.	Anticancer Res	32	3785-3790	2012
Wang W et al	E7050, a Met kinase inhibitor, reverses three different mechanisms of hepatocyte growth factor-induced resistance to tyrosine kinase inhibitors in *EGFR* mutant lung cancer cells.	Clin Cancer Res	18	1663-1671	2012

Koizumi H et al	Hsp90 inhibition overcomes HGF-triggering resistance to EGFR-TKIs in EGFR mutant lung cancer by decreasing client protein expression and angiogenesis.	J Thorac Oncol	7	1078-1085	2012
Yamada T et al	Hepatocyte growth factor induces resistance to anti-epidermal growth factor receptor antibody in lung cancer.	J Thorac Oncol	7	272-280	2012
Mihira H, Suzuki HI, Akatsu Y, Yoshimatsu Y, Igarashi T, Miyazono K, Watabe T	TGF-β-induced mesenchymal transition of MS-1 endothelial cells requires Smad-dependent cooperative activation of Rho signals and MRTF-A.	Journal of Biochemistry.	151	145-156	2012
Kawata M, Koinuma D, Ogami T, Umezawa K, Iwata C, Watabe T, Miyazono K	TGF-β-induced epithelial-mesenchymal transition of A549 lung adenocarcinoma cells is enhanced by pro-inflammatory cytokines derived from RAW 264.7 macrophage cells.	Journal of Biochemistry.	151	205-216	2012
Liersch R et al.	Induced lymphatic sinus hyperplasia in sentinel lymph nodes by VEGF-C as the earliest premetastatic indicator.	Int J Oncol.	41	2073-8	2012
Asai J et al.	Topical simvastatin accelerates wound healing in diabetes by enhancing angiogenesis and lymphangiogenesis.	Am J Pathol.	181	2217-2224	2012
Sasaki N et al.	A palmtop-sized microfluidic cell culture system driven by a miniaturized infusion pump.	Electrophoresis	33	1729-1735	2012
Okazaki et al.	Targeted overexpression of Angptl6/angiopoietin-related growth factor in theskin promotes angiogenesis and lymphatic enlargement in response to ultraviolet B.	J Dermatol.	39	366-374	2012
Aoi J et al.	A palmtop-sized microfluidic cell culture system driven by a miniaturized infusion pump.	Electrophoresis	33	1729-1735	2012

Majima Y et al.	Targeted overexpression of Angptl6/angiopoietin-related growth factor in theskin promotes angiogenesis and lymphatic enlargement in response to ultraviolet B.	Twist as a possible biomarker for metastatic basal cell carcinoma.	92	621-622	2012
Sato Y	The Vasohibin Family: A Novel Family for Angiogenesis Regulation.	J Biochem.	153	5-11	2013
Xue X, Gao W, Sun B, Xu Y, Han B, Wang F, Zhang Y, Sun J, Wei J, Lu Z, Zhu Y, Sato Y, Sekido Y, Miao Y, Kondo Y	Vasohibin 2 is transcriptionally activated and promotes angiogenesis in hepatocellular carcinoma.	Oncogene	32	1724-1734	2013
Koyanagi T, Saga Y, Takahashi Y, Suzuki Y, Suzuki M, Sato Y	Downregulation of vasohibin-2, a novel angiogenesis regulator, suppresses tumor growth by inhibiting angiogenesis in endometrial cancer cells.	Oncol Lett.	5	1058-1062	2013
Yazdani S, Miki Y, Tamaki K, Ono K, Iwabuchi E, Abe K, Suzuki T, Sato Y, Kondo T, Sasano H	Proliferation and maturation of intra-tumoral blood vessels in non-small cell lung cancer.	Human Pathol.	[Epub ahead of print]		2013
Kanomata N, Sato Y, Miyaji Y, Nagai A, Moriya T	Vasohibin-1 is a new predictor of disease-free survival in operated renal cell carcinoma patients.	J. Clin. Pathol.	[Epub ahead of print]		2013
Kosaka T, Miyazaki Y, Miyajima A, Mikami S, Hayashi Y, Tanaka N, Nagata H, Kikuchi E, Nakagawa K, Okada Y, Sato Y, Oya M	The prognostic significance of vasohibin-1 expression in patients with prostate cancer.	Br J Cancer	[Epub ahead of print]		2013
Sakimoto S et al	An angiogenic role for adrenomedullin in choroidal neovascularization.	PLoS One	8	e58096	2013
Yamakawa D et al	Ligand-independent Tie2 dimers mediate kinase activity stimulated by high dose Angiopoietin-1.	J Biol Chem	288	12469-12477	2013

Sawane M et al	Apelin inhibits diet-induced obesity by enhancing lymphatic and blood vessel integrity.	Diabetes			inpress
Matsui T et al	Possible role of mural cell covered mature blood vessels in inducing drug resistance in cancer-initiating cells.	Am J Pathol	182	1792-1799	2013
Jia W et al	Galectin-3 accelerates M2 macrophage infiltration and angiogenesis in tumors.	Am J Pathol	182	1821-1831	2013
Ishikawa D et al	mTOR inhibitors control erlotinib-resistance of *EGFR* mutant lung cancer cells triggered by HGF.	PLOS ONE		In press	2013
Sano T et al	Novel PI3K-mTOR inhibitor, BEZ235, circumvents erlotinib-resistance of EGFR mutant lung cancer cells triggering by HGF.	Int J Cancer		In press	2013
Yamada T et al	Scaffold Aki1, a novel therapeutic target for lung cancer with epidermal growth factor receptor mutations.	Oncogene		In press	2013
Nakagawa T et al	EGFR-TKI resistance due to *BIM* polymorphism can be circumvented by in combination with HDAC inhibition.	Cancer Res	73	2428-34	2013
Mitsuhashi A et al	Surfactant protein A suppresses lung cancer progression by regulating the polarization of tumor-associated macrophages.	Am J Pathol	182	1844-1853	2013
Miura K, Wakayama Y, Tanino M, Orba Y, Sawa H, Hatakeyama M, Tanaka S, Sabe H, Mochizuki N.	Involvement of EphA2-mediated tyrosine phosphorylation of Shp2 in Shp2-regulated activation of extracellular signal-regulated kinase.	Oncogene			2013 In press

Isolation of a small vasohibin-binding protein (SVBP) and its role in vasohibin secretion

Yasuhiro Suzuki[1], Miho Kobayashi[1], Hiroki Miyashita[1], Hideki Ohta[2], Hikaru Sonoda[2] and Yasufumi Sato[1,*]

[1]Department of Vascular Biology, Institute of Development, Aging, and Cancer, Tohoku University, 4-1 Seiryo-machi, Aoba-ku, Sendai 980-8575, Japan

[2]Discovery Research Laboratories, Shionogi and Company Limited, Osaka 567-0085, Japan

*Author for correspondence (y-sato@idac.tohoku.ac.jp)

Accepted 31 May 2010
Journal of Cell Science 123, 3094-3101

doi:10.1242/jcs.067538

Summary

Upon stimulation with angiogenic factors, vascular endothelial cells (ECs) secrete a negative-feedback regulator of angiogenesis, vasohibin-1 (VASH1). Because VASH1 lacks a classical signal sequence, it is not clear how ECs secrete VASH1. We isolated a small vasohibin-binding protein (SVBP) composed of 66 amino acids. The level of *Svbp* mRNA was relatively high in the bone marrow, spleen and testes of mice. In cultured ECs, *Vash1* mRNA was induced by VEGF, and *Svbp* mRNA was expressed constitutively. The interaction between VASH1 and SVBP was confirmed using the BIAcore system and immunoprecipitation analysis. Immunocytochemical analysis revealed that SVBP colocalized with VASH1 in ECs. In polarized epithelial cells, SVBP accumulated on the apical side, whereas VASH1 was present throughout the cells and partially colocalized with SVBP. Transfection of SVBP enhanced VASH1 secretion, whereas knockdown of endogenous SVBP markedly reduced VASH1 secretion. SVBP increased the solubility of VASH1 protein in detergent solution and inhibited the ubiquitylation of VASH1 protein. Moreover, co-transfection of SVBP significantly augmented the inhibitory effect of VASH1 on EC migration. These results indicate that SVBP acts as a secretory chaperone for VASH1 and contributes to the anti-angiogenic activity of VASH1.

Key words: Vasohibin, Secretion, Angiogenesis, Molecular chaperon, Ubiquitylation, Endothelial cell

Introduction

Angiogenesis is essential for physiological events, such as development, reproduction, and wound healing. It is also involved in various pathological processes, including tumor growth and ischemic retinopathy (Carmeliet, 2003). Angiogenesis is tightly regulated by stimulators, such as vascular endothelial growth factor (VEGF) and fibroblast growth factor-2 (FGF-2); angiogenesis inhibitors, such as angiostatin, endostatin and thrombospondin-1; and factors that modulate vascular maturation, such as angiopoietin-1 and transforming growth factor-β (Kerbel, 2008; Sato, 2006). Recently, ECs were shown to produce factors that regulate angiogenesis in an autocrine manner. The expression of Delta-like 4 and its cognate receptor Notch1 are detected mainly in tip cells and stalk cells, respectively, and contribute to their regulation during sprouting angiogenesis (Hellstrom et al., 2007; Leslie et al., 2007; Siekmann and Lawson, 2007).

We previously isolated the angiogenesis inhibitor, vasohibin-1 (VASH1), which is produced and secreted by vascular ECs upon stimulation by VEGF and FGF-2 (Hosaka et al., 2009; Kimura et al., 2009; Nasu et al., 2009; Sato et al., 2009; Sato and Sonoda, 2007; Shibuya et al., 2006; Shimizu et al., 2005; Tamaki et al., 2009; Wakusawa et al., 2008; Watanabe et al., 2004; Yamashita et al., 2006; Yoshinaga et al., 2008). VASH1 regulates EC proliferation and migration in an autocrine manner by acting as a negative-feedback regulator of angiogenesis. Purified VASH1 protein has been shown to inhibit the migration and network formation of human umbilical vein endothelial cells (HUVECs) in vitro. The administration of exogenous VASH1 strongly inhibits pathological and physiological angiogenesis without any significant side effects (Hosaka et al., 2009; Kimura et al., 2009; Shen et al., 2006; Watanabe et al., 2004; Yamashita et al., 2006). Most recently, we showed that VASH1 exhibits anti-lymphangiogenic activity and inhibits lymph node metastasis (Heishi et al., 2010). We also isolated VASH2, a homologue of VASH1 that displays more than 50% amino acid similarity to VASH1 (Kimura et al., 2009; Sato and Sonoda, 2007; Shibuya et al., 2006).

VASH1 protein is post-translationally processed into several truncated forms in ECs (Sato and Sonoda, 2007; Sonoda et al., 2006). Each VASH1 protein has at least two proteolytic cleavage sites in each terminus. Biochemical and functional analyses of VASH1 have revealed that some basic residues at the C-terminus are important for heparin binding and anti-angiogenic activity.

To elucidate the biological functions of VASH1 in detail, clarification of how newly synthesized VASH1 is secreted from ECs and acts on ECs is necessary. However, VASH1 protein does not contain a classical signal sequence typical of secreted proteins (Hegde and Kang, 2008). Also, it does not colocalize with the endoplasmic reticulum (ER) marker calnexin, suggesting that VASH1 might be transported and released into the extracellular space via an unconventional secretary pathway (Watanabe et al., 2004). In the present study, we characterized a VASH1 binding partner, which we designated small vasohibin-binding protein (SVBP), and determined a unique chaperone-like function for regulating VASH1 secretion.

Results

Isolation of the VASH1 binding factor

We performed yeast two-hybrid analysis to isolate potential VASH1 binding partner(s). Four strongly positive clones were obtained, each encoding hypothetical protein LOC374969 cDNA. This

hypothetical protein is also registered as coiled-coil domain containing 23 (CCDC23; GenBank accession number NP_955374). Because the protein is composed of only 66 amino acids, we named it small vasohibin-binding protein (SVBP). SVBP is highly conserved among mammals, and the amino acids corresponding to residues 32–52 are predicted to form a coiled-coil structure (Fig. 1A). Similarly to VASH1 and VASH2, SVBP does not have any classical signal sequences in the N-terminal region. We prepared recombinant human VASH1 (Watanabe et al., 2004), human VASH2 (Shibuya et al., 2006) and human SVBP proteins (Fig. 1B) and examined their direct interaction using the BIAcore system. SVBP bound strongly to VASH1 (K_D=3.1×10^{-8} M; Fig. 1C). We found that SVBP also bound to the VASH1 homologue, VASH2 (K_D =8.7×10^{-8} M; Fig. 1D).

Expression of *Svbp* mRNA in various organs and ECs

Because SVBP is a hypothetical protein, we performed Northern blot analysis to determine whether *Svbp* mRNA was actually expressed. The mouse EC line MS1 expressed a possible band of *Svbp* mRNA, and the intensity of this band was reduced by three different specific siRNAs (Fig. 2A). We also detected the expression of *Svbp* mRNA in various mouse organs (Fig. 2B). *Svbp* mRNA expression was especially high in the bone marrow, spleen and testes. We then evaluated changes in the expression of VASH1 and SVBP in ECs upon VEGF stimulation. As shown in Fig. 2C, a low level of *Vash1* mRNA was expressed under basal conditions, and it was induced by VEGF stimulation, as previously reported (Shimizu et al., 2005; Watanabe et al., 2004). By contrast, a high level of *Svbp* mRNA was expressed, even under basal conditions. These results, together with the steady state expression of SVBP in various organs, suggest that *Svbp* mRNA is expressed constitutively.

Interaction of SVBP and VASH1 in cultured ECs

We prepared mouse monoclonal antibodies against SVBP peptides (Asp2–Lys13). One of antibodies was able to detect recombinant SVBP protein by western blotting (Fig. 1B). Using this antibody, we tried to detect SVBP protein transiently expressed in MS1 cells. As shown in Fig. 3A, SVBP was detected in both the conditioned medium (CM) and cell lysate. The amount of SVBP in the CM was gradually increased in a time-dependent manner, implying that SVBP is constantly secreted in the medium. To characterize the interaction between VASH1 and SVBP, we performed co-immunoprecipitation followed by western blotting. Endogenous VASH1 was co-immunoprecipitated from both cell lysate and CM by the anti-SVBP antibody (Fig. 3B). We previously reported that the full-length VASH1 protein (44 kDa) is post-translationally truncated, resulting in at least three smaller forms (42 kDa, 36 kDa and 27 kDa) (Sonoda et al., 2006). Western blot analysis revealed that the 42 kDa protein was mainly detected in the cell lysate, whereas the 36 kDa and 27 kDa forms were detected in the CM, and all forms were co-immunoprecipitated with anti-SVBP antibody (Fig. 3B). We obtained similar results using MS1 cells transiently transfected with VASH1 and SVBP expression vectors (data not shown). Using the BIAcore system, we confirmed that SVBP bound to the 36 kDa (77–365) and 27 kDa (77–318) VASH1 proteins (Fig. 3C,D). We previously reported that proteolytic cleavage near Arg29 and Arg76 of VASH1 generates the two major forms of VASH1 (42 kDa and 36 kDa, respectively), and the subsequent proteolytic cleavage removing most of the basic region at the C-terminus generates the 27 kDa protein (Sonoda et al., 2006; Watanabe et al., 2004). These results suggest that de novo produced VASH1 and SVBP interact within cells and are secreted together, and this interaction might persist during the post-translational processing of VASH1.

Colocalization of SVBP and VASH1

Next, we transiently transfected human *VASH1* and *SVBP* cDNAs into MS1 cells and performed immunocytochemical analysis. The intracellular localization of VASH1 and SVBP was determined by immunostaining with VASH1- or SVBP-specific antibodies. SVBP partly colocalized with VASH1 within the cells (Fig. 4A). To further prove that the interaction between SVBP and VASH1 occurs inside the cell, we performed a Duolink in situ proximity ligation assay (PLA). This assay can detect protein–protein interactions using a combination of specific antibodies against them (Yamazaki et al., 2009). As shown in Fig. 4B, positive signals (red) were clearly observed by the treatment with both anti-VASH1 antibody and anti-Flag antibody (panel d), whereas there were no positive signals by the treatment with other combinations (panels a–c), indicating that SVBP and VASH1 do interact within a cell. Because ECs overlap each other in their peripheral cellular region when they are confluent and form a thin cellular sheet, it is very difficult to analyze the polarity as well as the subcellular localization of proteins within cells. Therefore, we used a polarized epithelial cell line (MDCK cells) as a model to observe the subcellular localization

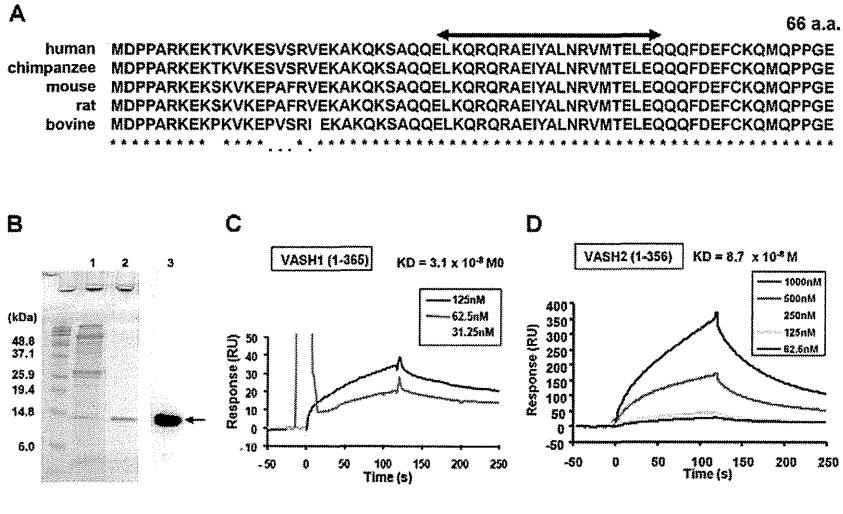

Fig. 1. Amino acid sequence of SVBP and physical interactions between SVBP and VASH1. (**A**) The SVBP protein is highly conserved among mammals. Asterisks and dots indicate identical and similar amino acids, respectively. The arrow indicates the putative coiled-coil domain. (**B**) Preparation of recombinant SVBP-Flag protein. SVBP-Flag protein was produced by a baculovirus system. The protein was purified by affinity chromatography using anti-FLAG antibody. 10 μl crude lysate (lane 1) and eluted sample from the column (lane 2) were subjected to SDS-PAGE followed by Coomassie Brilliant Blue staining. It was also confirmed that the purified recombinant protein could react with mouse monoclonal anti-SVBP antibody (lane 3). An arrow indicates SVBP-Flag. (**C**,**D**) Kinetic analysis of the direct binding of SVBP and VASH1 or VASH2 using the BIAcore system.

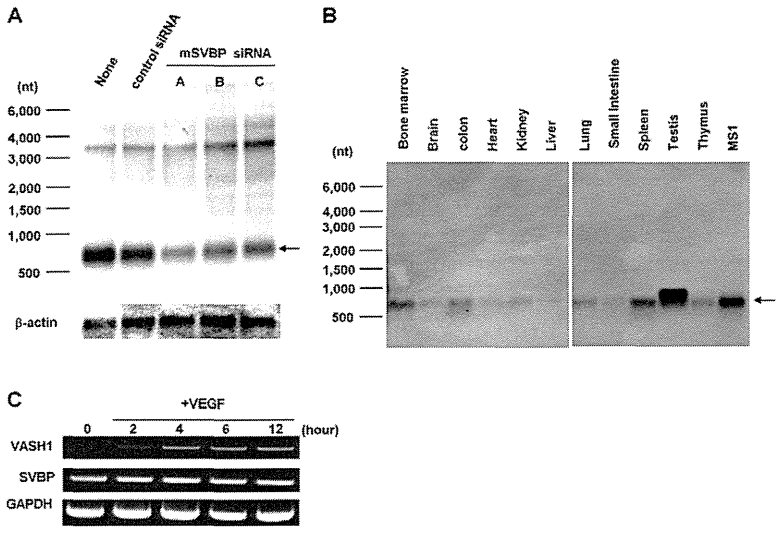

Fig. 2. In vitro and in vivo expression of *Svbp* and *Vash1* mRNA. (**A**) MS1 cells were transiently transfected with three different siRNAs designed for mouse ***Svbp*** mRNA and the expression evaluated by Northern blot. β-actin was used as an internal control. (**B**) ***Svbp*** mRNA (arrow) was extracted from the indicated adult mouse organs and analyzed by Northern blot. (**C**) MS1 cells pre-incubated in 0.1% FBS in α-MEM for 12 hours were stimulated with 20 ng/ml VEGF for the indicated periods. RT-PCR was performed on total RNA using specific primer pairs for mouse VASH1, SVBP and glyceraldehyde 3-phosphate dehydrogenase (GAPDH).

of VASH1 and SVBP in relation to cell polarity (Sabath et al., 2008). We confirmed that the tight junction marker ZO-1 was present at the apical side of MDCK cells (Fig. 4C). When VASH1 and SVBP cDNAs were co-transfected into MDCK cells, SVBP localized mainly on the apical side. This apical localization coincided with ZO-1. By contrast, VASH1 was present throughout the cell and partially colocalized with SVBP on the apical side (Fig. 4D). Positive signals of PLA were observed in the apical side of MDCK cells co-transfected with VASH1 and SVBP expression vectors (Fig. 4E), indicating that SVBP and VASH1 binds and colocalizes in the apical side of cells.

SVBP enhances VASH1 solubility and secretion

A previous report showed that VASH1 does not contain any classical signal sequence for translocation to the ER and does not colocalize with the ER marker calnexin (Watanabe et al., 2004). The above evidence that SVBP interacts with VASH1 both intracellularly and extracellularly prompted us to evaluate whether SVBP might affect VASH1 secretion. We transfected equal amounts of VASH1 expression vector and increasing amounts of SVBP expression vector into MS1 cells and found that SVBP enhanced the secretion of VASH1 in a dose-dependent manner (Fig. 5A). This increased secretion of VASH1 by SVBP was confirmed by ELISA, which measured the concentration of the VASH1–SVBP complex (Fig. 5B). Moreover, we confirmed that Brefeldin A, an inhibitor of ER- and Golgi-dependent secretory transport (Nickel, 2007; Seelenmeyer et al., 2003), does not affect the secretion of VASH1 (Fig. 5B), suggesting that VASH1 might be released from ECs via an unconventional secretion pathway (Nickel and Rabouille, 2009). We also observed that SVBP enhanced the secretion of VASH2, which also lacks a signal sequence (Fig. 5C). Furthermore, the interaction between VASH1 and SVBP dramatically changed the ability to extract VASH1 protein into 1% Triton X-100 cell lysis buffer (Fig. 5A). SVBP increased the amount of VASH1 in the soluble fraction, which coincided with a decrease of VASH1 in the insoluble fraction. The solubility of β-actin, an internal control, was not affected by SVBP. When endogenous SVBP was knocked down by siRNA, we observed the

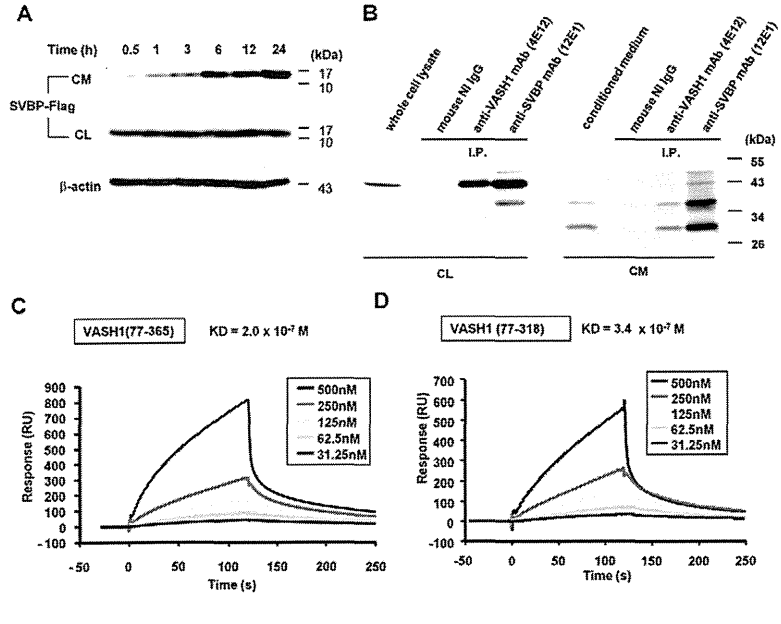

Fig. 3. SVBP–VASH1 complexes in the cell lysate and CM. (**A**) Time-course of SVBP release from ECs. MS1 cells transiently transfected with p3xFLAG-SVBP for 24 hours were washed with serum-free α-MEM, and then cultured in 0.1% FBS in α-MEM for the indicated periods. Concentrated CM and Cell lysate (CL) were evaluated by western blot. (**B**) Co-immunoprecipitation of the SVBP–VASH1 protein complex from HUVECs. CL from confluent HUVECs and their CM were immunoprecipitated with either anti-human VASH1 antibody or anti-human SVBP antibody as indicated. Immunoprecipitates were analyzed by western blot analysis using peroxidase-conjugated anti-human VASH1 antibody. IP, immunoprecipitation. (**C**,**D**) Kinetic analysis of the direct binding between SVBP and truncated forms of VASH1 using the BIAcore system.

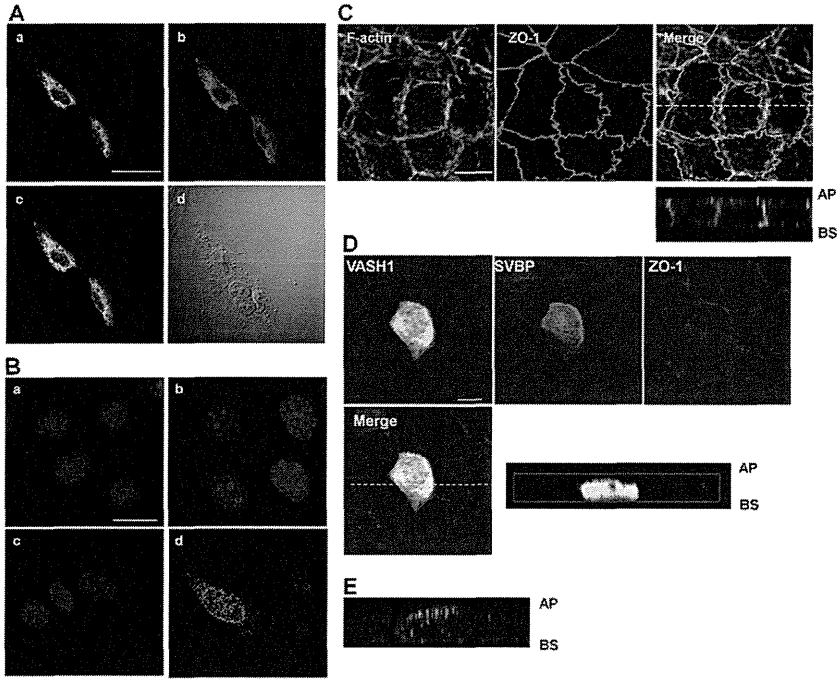

Fig. 4. Intracellular colocalization of SVBP and VASH1. (**A**) Colocalization of SVBP and VASH1 in MS1 cells transiently transfected with a human VASH1 expression vector and p3xFLAG-SVBP for 24 hours. The fixed cells were immunostained with anti-VASH1 (green) and anti-SVBP (red) antibodies. a, VASH1; b, SVBP; c, merge; d, DIC. Scale bar: 50 μm. (**B**) Interaction between SVBP and VASH1 in ECs. PLA was performed after incubation with combination of antibodies. a, normal mouse IgG + normal rabbit IgG; b, normal mouse IgG + anti-Flag antibody; c, anti-VASH1 mAb + normal rabbit IgG; d, anti-VASH1 mAb + anti-Flag antibody. Scale bar: 20 μm. (**C**) MDCK cells with polarization. MDCK cells immunostained with anti-ZO-1 (red, a marker of tight junction) and Phalloidin-FITC (green). Scale bar: 10 μm. (**D**) Apical localization of SVBP in polarized epithelial cells. MDCK cells were transiently co-transfected with human VASH1 and p3xFLAG-SVBP expression vectors for 24 hours. The fixed cells were immunostained with anti-VASH1 (green), anti-FLAG (red) and anti-ZO-1 (blue) antibodies. Scale bar: 10 μm. (**E**) Interaction between SVBP and VASH1 in the apical side of MDCK cells. MDCK cells transiently transfected with human VASH1 and p3xFLAG-SVBP expression vectors were subjected to PLA. AP, apical side; BS, basolateral side.

opposite results (Fig. 5D). SVBP expression did not affect *Vash1* mRNA levels (data not shown), and *Svbp* siRNA specifically decreased endogenous *Svbp* mRNA levels with no effect on the levels of *Vash1* mRNA (Fig. 5E). Also, *Svbp* siRNA decreased the ability to extract VASH1 protein into 1% Triton X-100 cell lysis buffer and decreased the secretion of VASH1 into the medium. These results indicate that SVBP has an important role in VASH1 secretion, probably by increasing the solubility of the VASH1 protein.

SVBP prevents ubiquitylation of VASH1

The solubility of some proteins in detergent solution is closely concerned with protein folding regulated by interactions with molecular chaperones (Dou et al., 2003; Muchowski et al., 2000). In general, misfolded or unfolded proteins are either refolded by molecular chaperones or degraded immediately by the ubiquitin proteasome system (UPS) (Hishiya and Takayama, 2008; Muchowski et al., 2000), which is known as an intrinsic protein quality control. We hypothesized that SVBP might contribute to the quality control of VASH1 protein in ECs. Therefore, we examined first whether the UPS affects VASH1 stability in ECs. To detect the total amount of VASH1 protein, we prepared cell lysate using 1% SDS cell lysis buffer, which was different to levels in the experiments performed in Fig. 5. As shown in Fig. 6A,B, the

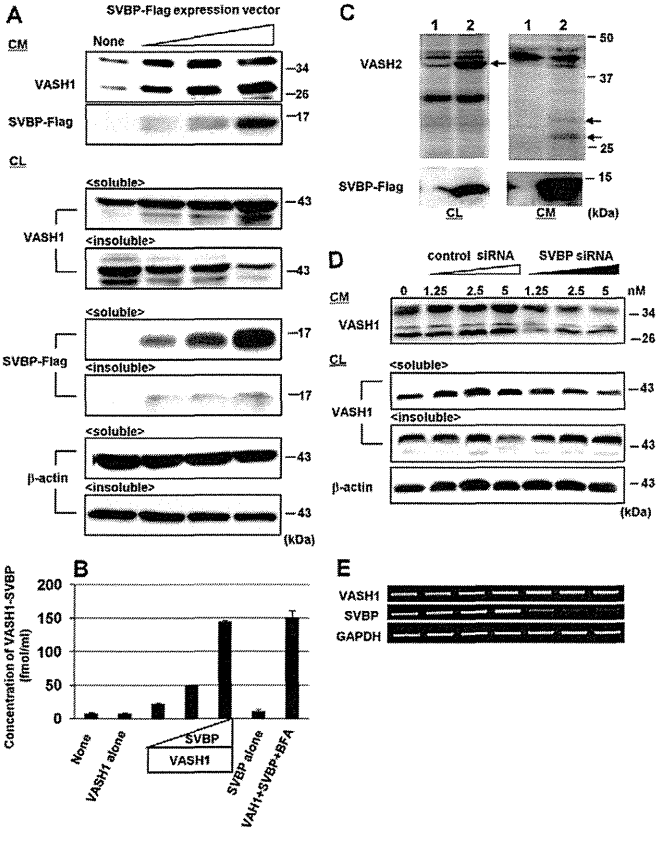

Fig. 5. SVBP increases VASH1 solubility and secretion. (**A**) CM was collected from MS1 cells transiently co-transfected with human VASH1 and various amounts of p3xFLAG-SVBP expression vectors after 24 hours. Concentrated CM, the supernatant (soluble fraction) of cell lysates (CL) and the pellet (insoluble fraction) were evaluated by western blot. (**B**) Measurement of the VASH1–SVBP complex in the CM. The CM was collected from transfected MS1 cells. The concentration of VASH1–SVBP complex in the CM was measured by ELISA. Error bars indicate s.d. BFA, Brefeldin A. (**C**) CL and concentrated CM of MS1 cells transfected with human VASH2 and/or p3xFLAG-SVBP expression vectors were prepared and subjected to western blot analysis. Arrows indicate VASH2 protein in CL or its truncated forms in CM. (**D**) Western blot analysis showed that SVBP knockdown decreases VASH1 secretion and solubility. Concentrated CM and soluble and insoluble fractions of CLs were prepared 48 hours after *VASH1*-expressing MS1 cells were transfected with various concentrations of siRNAs designed against mouse *Svbp* mRNA. (**E**) RT-PCR shows that SVBP knockdown does not affect *Vash1* expression in MS1 cells.

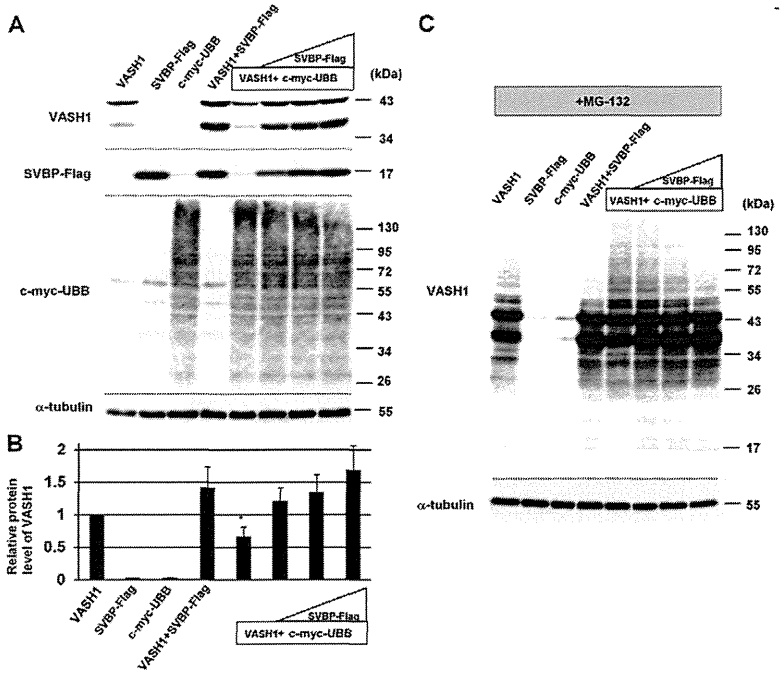

Fig. 6. SVBP inhibits the ubiquitylation of VASH1. (**A**) MS1 cells were transiently transfected with human VASH1, 3xFLAG-SVBP and Myc-UBB expression vectors in the indicated combinations. Cell lysates were prepared and subjected to western blot analysis 24 hours after transfection. (**B**) Densitometric quantification of VASH1 protein. The relative VASH1 protein levels were normalized to α-tubulin. Error bars indicate s.d. (n=3). *P=0.05 versus VASH1 alone. (**C**) Western blot of MS1 cells transiently transfected identically to those in A, but 6 hours after transfection, the cells were incubated with 10 μM MG132 for 18 hours and harvested with cell lysis buffer containing ubiquitin aldehyde.

total amount of VASH1 protein was reduced in the presence of Myc–ubiquitin-B (UBB) compared with VASH1 alone. By contrast, this reduction was recovered in a dose-dependent manner by co-transfection with SVBP, implying that the VASH1 protein is stable when associated with SVBP. In the presence of a proteasome inhibitor, MG-132, polyubiquitylated VASH1 proteins were detected as many ladder bands of a higher molecular mass than the 42 kDa form (Fig. 6C). Co-transfection with SVBP dramatically reduced these polyubiquitylated VASH1 proteins. These results suggest that the interaction between SVBP and VASH1 enhances the stability of VASH1 protein by preventing ubiquitylation.

SVBP accelerates VASH1 function

Finally, we examined whether SVBP affects the anti-angiogenic activity of VASH1. The co-expression of SVBP and VASH1 significantly inhibited VEGF-inducible EC migration (Fig. 7A). Stimulation with VEGF (20 ng/ml) increased MS1 migration 2.2-fold relative to control cells. MS1 cells transfected with VASH1 no longer responded to VEGF stimulation. Co-transfection with VASH1 and SVBP downregulated the basal level of EC migration compared with other samples, regardless of VEGF stimulation. We then examined whether this anti-angiogenic activity might be derived from secreted VASH1. The CM from MDCK cells transfected with VASH1 and/or SVBP expression vector was added to HMVECs. As shown in Fig. 7B, VEGF-inducible migration of HMVECs was inhibited by CM containing the VASH1–SVBP complex in a concentration-dependent manner. These results indicate that SVBP regulates the secretion of VASH from ECs and contributes to the anti-angiogenic activity of VASH1.

Discussion

Secretory proteins generally contain a typical signal sequence composed of successive hydrophobic amino acids that is usually located in the N-terminal region and removed by signal peptidase after the protein passes through the ER membrane (Hegde and Kang, 2008). VASH1 has no such classical secretion signal sequence (Watanabe et al., 2004), and does not colocalize with the ER marker calnexin in ECs (Watanabe et al., 2004). These observations led us to hypothesize that de novo produced VASH1 might be secreted via an unconventional secretory pathway. Here, we identified SVBP as a novel VASH1 binding partner. The association between endogenous SVBP and VASH1 proteins in cell lysate and CM of ECs appeared crucial for VASH1 secretion, because knockdown of SVBP significantly impaired VASH1 secretion. We also showed that SVBP bound to VASH2 and enhanced its secretion from ECs. The expression of *VASH1* mRNA is induced by VEGF or FGF-2, mediated by protein kinase C-δ downstream of VEGF receptor-2 (Shimizu et al., 2005). However, we observed a constitutive expression of *Svbp* mRNA in ECs

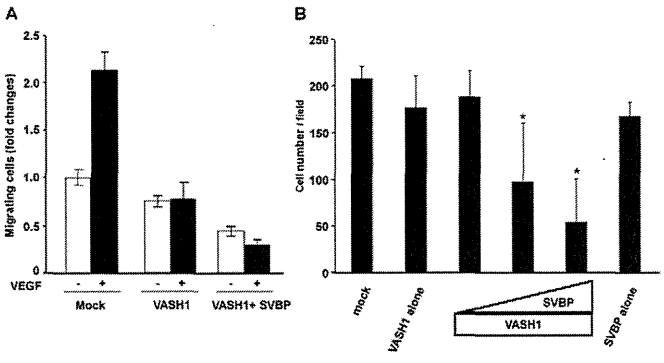

Fig. 7. SVBP accelerates VASH1-mediated inhibition of EC migration. (**A**) MS1 cells were transiently transfected with human VASH1 and/or 3xFLAG-SVBP expression vectors and cell migration analyzed with a modified Boyden chamber assay. Relative numbers of migrating cells are shown as mean ± s.d. (n=3). (**B**) HMVECs were treated with CM collected from MDCK cells transfected human VASH1 and various amounts of p3xFLAG-SVBP expression vectors. Cell migration was analyzed with a modified Boyden chamber assay. The numbers of migrating cells in a field are shown as mean ± s.d. (n=9). *P<0.001 versus negative control (mock).

under basal conditions and in various normal mouse organs. Thus, the scenario of VASH1 secretion might be as follows: SVBP is prepared in advance and accumulates under or on the cell surface. Once VASH1 has been induced, it binds SVBP, which facilitates the secretion of VASH1 (Fig. 8). The molecular mechanism by which VASH1 exhibits anti-angiogenic activity is not fully understood. Co-transfection of VASH1 and SVBP to ECs decreased the basal migration of ECs, suggesting that anti-angiogenic activity of VASH1 might not simply be caused by the blockade of VEGF-mediated signaling in ECs. We predict a putative receptor for VASH1, which transduces specific signals for anti-angiogenesis in ECs. If we could isolate such a receptor, it should help us to characterize the molecular mechanism of VASH activity.

Molecular chaperones comprise several highly conserved families, including heat shock proteins (HSPs), and contribute to post-translational quality control of proteins (Wickner et al., 1999). Although the native structure of a protein is determined principally by its amino acid sequence, the process of folding in vivo often requires the assistance of molecular chaperones, which are often required to maintain the proper conformation of proteins under changing environmental conditions. Misfolded or unfolded proteins exhibit insolubility in detergent solution. Some molecular chaperones can help such proteins to complete the correct folding and recover solubility. For instance, HSP70 and HSP90 are reported to function as molecular chaperones for microtubule-associated protein Tau or endothelial nitric oxide synthase and increase their solubility in detergent solution (Dou et al., 2003; Jiang et al., 2003; Petrucelli et al., 2004). Because SVBP non-covalently binds VASH1 and increases its solubility in 1% Triton X-100 (a nonionic detergent) cell lysis buffer, SVBP might have a chaperone-like role for VASH1. Molecular chaperones, including HSPs, generally accumulate on membranes (Horvath et al., 2008), and our data show that SVBP accumulates on the apical plasma membrane of polarized epithelial cells, supporting a chaperone-like function of SVBP.

Leaderless secretory proteins (e.g. FGF-2, interleukin-1β and galectins) are released from a variety of cell types via unconventional secretory pathways independently of the ER and Golgi (Calderwood et al., 2007; Hughes, 1999; Keller et al., 2008; Nickel, 2005; Nickel and Rabouille, 2009; Piotrowicz et al., 1997; Torrado et al., 2009). Four potential mechanisms of unconventional protein export have been proposed: export across the plasma membrane, export by secretory lysosomes, export through the release of exosomes derived from multivesicular bodies, and export mediated by plasma membrane shedding of microvesicles (Nickel, 2005; Nickel and Rabouille, 2009). Piotrowicz and colleagues previously reported that the molecular chaperone HSP27 binds to FGF-2 in ECs, which facilitates FGF-2 secretion from ECs via an unconventional secretory pathway (Piotrowicz et al., 1997). Importantly, a recent report showed that correctly folded FGF-2 might be required for translocation across the plasma membrane (Torrado et al., 2009). Interestingly, HSPs themselves lack a secretion signal sequence but are released from cells and function as extracellular ligands, giving rise intracellular signaling (Calderwood et al., 2007). However, the detailed mechanism by which molecular chaperones modulate the secretion of leaderless secretory proteins remains obscure. Further study is required to determine whether SVBP is involved in the secretion of other leaderless proteins such as FGF-2.

Recently, the level of *Ccdc23* (also known as SVBP) mRNA was shown to be significantly higher in adenomatous polyposis coli than in normal colorectal mucosa (Gaspar et al., 2008), but the expression of VASH1 appears to be restricted to ECs. Thus, the expression of *Svbp* mRNA might not always associate with the expression of *Vash1* mRNA. SVBP might have additional role(s) beyond that of a VASH1 binding partner. This possibility is currently under investigation.

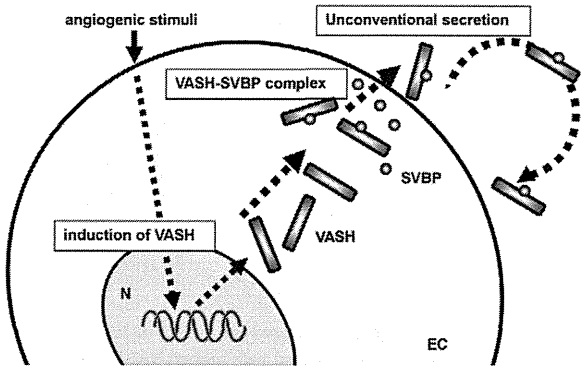

Fig. 8. SVBP facilitates VASH1 secretion by acting as a chaperone. SVBP is constitutively expressed, whereas VASH1 is induced by angiogenic factors (e.g. VEGF and FGF-2) in ECs. SVBP might bind to de novo produced VASH1 and render it soluble via chaperone-like activity, resulting in the efficient secretion of the VASH–SVBP complex into the extracellular space. N, nucleus.

Materials and Methods

Yeast two-hybrid screen

We performed a yeast two-hybrid screen to isolate VASH1 binding partners as previously described (Colland et al., 2004). Full-length human VASH1 (amino acids 1–365) and the human placental random-primed cDNA library were used as bait and prey, respectively. We screened 1.3×10^8 independent clones. The prey fragments of the positive clones were amplified by polymerase chain reaction (PCR) and sequenced. The resulting sequences were used to identify the corresponding gene in the GenBank database.

Plasmid construction

Human *SVBP* cDNA (CCDC23; GenBank accession number NM_199342) was cloned into the *NotI* and *XbaI* sites of the p3xFLAG-CMV14 plasmid vector (Sigma) to generate p3xFLAG-SVBP, in which *SVBP* cDNA was attached to a triple repeat of the FLAG tag sequence at the 3′ end. The DNA fragment containing the *SVBP* cDNA joined with 3xFLAG was cloned into the *SmaI* site of baculovirus transfer vector pYNG (Katakura). Human ubiquitin B cDNA (UBB; GenBank accession number NM_018955) was cloned into the *EcoRI* site of the pCMV Myc plasmid vector (Clontech) to generate pCMV Myc-UBB, in which *UBB* cDNA was attached to a Myc sequence at the 5′ start site.

Evaluation of molecular interactions using the BIAcore system

Recombinant human SVBP-FLAG protein was expressed in the silkworm, *Bombyx mori*, as previously reported (Takahashi et al., 2007). Briefly, the constructed transfer vector was mixed with cysteine-proteinase-deleted baculoviral genomic DNA and then co-transfected in BmN cells of *B. mori* larvae. The resulting recombinant baculovirus was infected in *B. mori* pupae. Harvested pupae were lysed and the SVBP-FLAG protein purified using an anti-FLAG M2 affinity column (Sigma). Purified recombinant full-length VASH1, its truncated forms and VASH2 proteins were prepared as previously described (Shibuya et al., 2006; Sonoda et al., 2006; Watanabe et al., 2004). The interaction of VASH1 and VASH2 with SVBP was analyzed using a BIAcore 3000 (BIAcore AB). SVBP (20.6 μg/ml) in 10 mM sodium acetate (pH 4.5) was immobilized on a CM5 sensor chip using the amine-coupling method according to the manufacturer's protocol. VASH1, its truncated forms, or VASH2 in 10 mM HEPES (pH 7.4), 0.15 M NaCl, 3 mM EDTA, 0.005% Surfactant P20 (pH 7.4) at concentrations of 62.5 nM to 1 μM was passed over the surface of the sensor chip at a flow rate of 20 μl/minute. The interaction was monitored as the change in surface plasmon resonance response at 25°C. After 2 minutes of monitoring, the same buffer was introduced to the sensor chip in place of the VASH1 solution to start the dissociation. The sensor surface was regenerated with 10 mM glycine (pH 2.0) at the end of each experiment. Both the association rate constant (K_a) and the dissociation rate constant (K_d) were calculated according to the BIAevaluation software. The dissociation constant (K_D) was determined as K_d/K_a.

Cell culture

The murine EC line MS1 was cultured in α minimal essential medium (αMEM; Wako Pure Chemical) supplemented with 10% fetal bovine serum (FBS; JRH Biosciences) (Arbiser et al., 1997). Polarized epithelial Madin-Darby canine kidney (MDCK) cells were cultured in Dulbecco's modified Eagle medium (Wako Pure Chemical) supplemented with 10% FBS (Martin-Belmonte et al., 2001). Human umbilical vein endothelial cells (HUVECs) and human microvascular endothelial cells (HMVECs) were purchased from KURABO and cultured on type I-C collagen-coated dishes (Asahi Techno Glass) in endothelial basal medium containing 5% FBS and EC growth supplements (Cambrex Bio Science Walkersville).

RT-PCR

Total RNA was extracted from cultured cells using the RNeasy Mini Kit (Qiagen). RT-PCR was carried out using the First Strand cDNA Synthesis Kit (Roche Diagnostics) according to the manufacturer's instructions. Briefly, total RNA was reverse transcribed for 50 minutes at 42°C using oligo(dT) primers. PCR was performed using sets of primers specific for the target genes. Thermal cycler conditions were 20–30 cycles of 94°C for 15 seconds for denaturing, 56°C for 30 seconds for annealing and 72°C for 45 seconds for extension. PCR products were separated on a 1.5% agarose gel and visualized under ultraviolet by ethidium bromide staining. The primer pairs were as follows: mouse *Ccdc23*, sense (5′-ATGGATCCACCTGCCCGGAA-3′) and antisense (5′-TCACTCCCCAGGCGGCTGCA-3′); mouse *Vash1*, sense (5′-ATGTG-GAAGGCATGTGGCCAAG-3′) and antisense (5′-CACCCGGATCTGGTACC-CACT-3′).

Northern blotting

Total RNA was isolated from cultured cells or mouse organs using QIAzol reagent (Qiagen), and mRNA was isolated from total RNA samples using Oligotex-dT30 Super (Takara) according to the manufacturers' instructions. Each mRNA sample (600 ng) was separated by 1% agarose-formaldehyde gel electrophoresis and transferred to a positively charged nylon membrane (Roche Diagnostics). Membranes were hybridized with antisense SVBP- or β-actin-specific RNA probes labeled with digoxigenin (DIG) using the SP6/T7 DIG RNA Labeling Kit (Roche Diagnostics). Hybridization was performed for 2 hours at 68°C using PerfectHyb reagent (Toyobo) containing 0.2 ng/ml DIG-labeled antisense RNA probe. After hybridization, the membranes were washed twice with 2× SSC, 0.1% sodium dodecyl sulfate (SDS) at 68°C for 15 minutes. The final wash was performed twice using 0.1× SSC, 0.1% SDS at 68°C for 15 minutes. The mRNA bands were detected using the Northern Blot Starter Kit (Roche Diagnostics), and the results were analyzed using a LAS-4000 (Fuji Photo Film).

Small interfering RNAs (siRNAs)

Three sets of specific siRNAs targeting mouse *Svbp* mRNA (mouse CCDC23; GenBank accession number NM_024462) were designed and synthesized by Invitrogen. The target sequences were: *Svbp* siRNA A, 5′-GGGUCAGAGCUAAC-CAAGAAGCAUU-3′; *Svbp* siRNA B, 5′-AAGAAGCAUUCAGAAGCCAAAC-CAU-3′; *Svbp* siRNA C, 5′-GAGAUCUAUGCUCUCAACAGAGUCA-3′. Stealth RNAi Negative Control Low GC Duplex (Invitrogen) was used as a negative control. Cells were cultured to 60–70% confluency and transfected with *Svbp* siRNAs using Lipofectamine RNAiMAX (Invitrogen) according to the manufacturer's instructions. The medium was changed after 3 hours of transfection and the cells cultured for an additional 24–48 hours.

Transient transfection

MS1 and MDCK cells were transiently transfected with human VASH1 (Watanabe et al., 2004), human VASH2 (Shibuya et al., 2006), p3xFLAG-SVBP, and pCMV Myc-UBB expression vectors using Effectene reagent (Qiagen) according to the manufacturer's instructions.

Preparation of anti-SVBP monoclonal antibodies

A/J mice (Japan SLC) were immunized three times with Cys-SVBP peptide (Asp2–Lys13 of the CCDC23 protein) conjugated to keyhole limpet hemocyanin. Spleen cells from the immunized mice were fused with the myeloma cell line P3U1. Culture supernatant from each hybridoma was screened as previously described (Ohta et al., 1999; Watanabe et al., 2004). Positive hybridomas were cloned using the limiting-dilution technique. The resulting monoclonal antibodies (mAbs) were purified from ascites using protein-A–Sepharose beads (GE Healthcare Bio-Sciences).

Western blotting

Cells were lysed in 1% SDS cell lysis buffer consisting of 10 mM Tris-HCl, pH 7.5, 150 mM NaCl, 1% SDS supplemented with 0.5 mM phenylmethylsulfonyl fluoride and Complete EDTA-free Protease Inhibitor Cocktail (Roche Diagnostics). The CM was concentrated 50-fold using an Amicon Ultra-15 (10,000 MWCO; Millipore). Equal amounts of protein from cell lysates and concentrated CM were separated by SDS-polyacrylamide gel electrophoresis (SDS-PAGE) and transferred onto polyvinylidene fluoride (PVDF) membranes (Bio-Rad). Blotting was performed according to standard procedures. The primary antibodies were anti-human VASH1 mAb (Watanabe et al., 2004), anti-human VASH2 mAb (Shibuya et al., 2006), anti-human SVBP mAb, anti-FLAG M2 mAb (Sigma), and anti-Myc mAb (Clontech). Normalization was performed using anti-β-actin mAb (Sigma). Immunoreactive protein bands were detected using ECL Western Blotting Detection Reagents (GE Healthcare) or Immobilon Western HRP Substrate (Millipore) using an LAS-4000 (Fuji Photo Film). Densitometric quantification was performed using Multi Gauge Ver 3.0 software (Fuji Photo Film).

Extraction of soluble and insoluble VASH1 proteins from cultured cells

Cells were lysed in ice-cold 1% Triton X-100 cell lysis buffer consisting of 10 mM Tris-HCl, pH 7.5, 150 mM NaCl, 1% sodium deoxycholate, 0.1% SDS, and 1% Triton X-100. Cell extracts were placed on ice for 1 hour and then centrifuged at 15,000 ***g*** for 15 minutes to separate the supernatant (soluble fraction) and pellet (insoluble fraction). The insoluble fraction was washed three times with ice-cold 1% Triton X-100 cell lysis buffer and re-extracted with sample buffer for SDS-PAGE. Western blotting was carried out as described above.

Immunoprecipitation

The cell lysate or CM was incubated with anti-human VASH1 antibody, anti-human SVBP antibody, or normal mouse IgG (Santa Cruz Biotechnology) at 4°C overnight on a rotating mixer. Protein-A–Sepharose beads were then added and the samples incubated for another 2 hours at 4°C. The beads were washed three times with phosphate-buffered saline (PBS) containing 0.05% Tween 20. Immunoprecipitated proteins were eluted into sample buffer for SDS-PAGE, and western blotting was performed as described above.

Immunostaining

Transfected MS1 or MDCK cells were fixed in 4% paraformaldehyde, permeabilized with 0.1% Triton-X100, and stained with VASH1, SVBP, FLAG (Sigma), ZO-1 (Sanko Junyaku) antibodies, or Phalloidin-FITC (Sigma). Nuclei were visualized using TO-PRO®3 (Invitrogen). All incubations were performed at 4°C in PBS containing 1% bovine serum albumin. Images were captured using a Fluoview FV1000 confocal microscope system (Olympus).

Duolink in situ proximity ligation assay (PLA)

The Duolink in situ PLA kit was purchased from Olink Bioscience. Transfected MS1 cells and MDCK cells were immunoreacted with the combination of anti-human VASH1 mAb (mouse), anti-FLAG plyclonal Ab (rabbit), normal mouse IgG, and normal rabbit IgG as described above. According to the manufacturer's protocol, a pair of anti-mouse MINUS and anti-rabbit PLUS was used to generate positive fluorescence signals indicating that two PLA probes bound in close proximity (<40 nm). Nuclei counterstaining using TO-PRO®3 and the images were captured as described above.

ELISA for VASH1-SVBP complex

We established a highly sensitive ELISA system that could quantify the VASH1–SVBP complex. A pair of specific monoclonal antibody against SVBP and VASH1 was used to coat a 96-well plate and for HRP labeling, respectively. MS1 cells and MDCK cells were transiently co-transfected with a combination of human VASH1 and SVBP expression vectors for 6 hours, then were washed with serum free α-MEM, and cultured in 0.1% FBS in α-MEM for 24 hours. The CMs were centrifuged at 5000 ***g*** for 15 minutes to remove cell debris. Subsequently, the supernatant was subjected to ELISA. The detailed procedure for the measurements carried out is described elsewhere (Heishi et al., 2010).

Endothelial cell migration

The migratory activity of ECs was measured by modified Boyden chamber assay in two different procedures (Kobayashi et al., 2006; Watanabe et al., 2004). First, transfected MS1 cells were plated on the upper chambers (inserts) of the Boyden chamber (8.0 μm pore size, Corning). The lower chamber was filled with 0.2% FBS in α-MEM with or without 20 ng/ml recombinant human VEGF (Sigma). After incubation for 18 hours, cells that migrated to the lower surface of the membrane were fixed with 4% formaldehyde, stained with crystal violet (Sigma), and counted in a blinded manner. The relative number of migrating cells was calculated; the mean number of migrating cells transfected with empty vector (mock) alone was set equal to 1.0.

Another procedure was prepared to evaluate anti-angiogenic activity of the VASH1–SVBP complex secreted from cells. MDCK cells were transiently co-transfected with a combination of human VASH1 and SVBP expression vectors for 6 hours, washed with serum free α-MEM and then cultured in 0.05% FBS in α-MEM for 24 hours. CM was concentrated 10-fold using an Amicon Ultra-15. HMVECs, preincubated in 0.5% FBS in Medium-199 (Invitrogen) for 16 hours, were suspended in concentrated CMs and then plated on the upper chambers of the Boyden chamber. The lower chamber was filled with 0.5% FBS in Medium-199 with 20 ng/ml recombinant human VEGF. HMVECs were allowed to migrate under VEGF stimulation for 4 hours. The number of cells that migrated across the filter was counted in nine fields per insert in a blinded manner.

Statistical analysis

Data are expressed as mean ± s.d. Significance was assessed by one-way analysis of variance (ANOVA) followed by Sheffe's *t*-test.

This study was supported by the Grant-in-Aid for Scientific Research on Priority Areas (17014006) and the Grant-in-Aid for Young Scientists (19790509) from the Ministry of Education, Culture, Sports, Science, and Technology of Japan.

References

Arbiser, J. L., Moses, M. A., Fernandez, C. A., Ghiso, N., Cao, Y., Klauber, N., Frank, D., Brownlee, M., Flynn, E., Parangi, S. et al. (1997). Oncogenic H-ras stimulates tumor angiogenesis by two distinct pathways. *Proc. Natl. Acad. Sci. USA* **94**, 861-866.

Calderwood, S. K., Mambula, S. S. and Gray, P. J., Jr (2007). Extracellular heat shock proteins in cell signaling and immunity. *Ann. NY Acad. Sci.* **1113**, 28-39.

Carmeliet, P. (2003). Angiogenesis in health and disease. *Nat. Med.* **9**, 653-660.

Colland, F., Jacq, X., Trouplin, V., Mougin, C., Groizeleau, C., Hamburger, A., Meil, A., Wojcik, J., Legrain, P. and Gauthier, J. M. (2004). Functional proteomics mapping of a human signaling pathway. *Genome Res.* **14**, 1324-1332.

Dou, F., Netzer, W. J., Tanemura, K., Li, F., Hartl, F. U., Takashima, A., Gouras, G. K., Greengard, P. and Xu, H. (2003). Chaperones increase association of tau protein with microtubules. *Proc. Natl. Acad. Sci. USA* **100**, 721-726.

Gaspar, C., Cardoso, J., Franken, P., Molenaar, L., Morreau, H., Moslein, G., Sampson, J., Boer, J. M., de Menezes, R. X. and Fodde, R. (2008). Cross-species comparison of human and mouse intestinal polyps reveals conserved mechanisms in adenomatous polyposis coli (APC)-driven tumorigenesis. *Am. J. Pathol.* **172**, 1363-1380.

Hegde, R. S. and Kang, S. W. (2008). The concept of translocational regulation. *J. Cell Biol.* **182**, 225-232.

Heishi, T., Hosaka, T., Suzuki, Y., Miyashita, H., Oike, Y., Takahashi, T., Nakamura, T., Arioka, S., Mitsuda, Y., Takakura, T. et al. (2010). Endogenous angiogenesis inhibitor vasohibin1 exhibits broad-spectrum antilymphangiogenic activity and suppresses lymph node metastasis. *Am. J. Pathol.* **176**, 1950-1958.

Hellstrom, M., Phng, L. K., Hofmann, J. J., Wallgard, E., Coultas, L., Lindblom, P., Alva, J., Nilsson, A. K., Karlsson, L., Gaiano, N. et al. (2007). Dll4 signalling through Notch1 regulates formation of tip cells during angiogenesis. *Nature* **445**, 776-780.

Hishiya, A. and Takayama, S. (2008). Molecular chaperones as regulators of cell death. *Oncogene* **27**, 6489-6506.

Horvath, I., Multhoff, G., Sonnleitner, A. and Vigh, L. (2008). Membrane-associated stress proteins: more than simply chaperones. *Biochim. Biophys. Acta* **1778**, 1653-1664.

Hosaka, T., Kimura, H., Heishi, T., Suzuki, Y., Miyashita, H., Ohta, H., Sonoda, H., Moriya, T., Suzuki, S., Kondo, T. et al. (2009). Vasohibin-1 expression in endothelium of tumor blood vessels regulates angiogenesis. *Am. J. Pathol.* **175**, 430-439.

Hughes, R. C. (1999). Secretion of the galectin family of mammalian carbohydrate-binding proteins. *Biochim. Biophys. Acta* **1473**, 172-185.

Jiang, J., Cyr, D., Babbitt, R. W., Sessa, W. C. and Patterson, C. (2003). Chaperone-dependent regulation of endothelial nitric-oxide synthase intracellular trafficking by the co-chaperone/ubiquitin ligase CHIP. *J. Biol. Chem.* **278**, 49332-49341.

Keller, M., Ruegg, A., Werner, S. and Beer, H. D. (2008). Active caspase-1 is a regulator of unconventional protein secretion. *Cell* **132**, 818-831.

Kerbel, R. S. (2008). Tumor angiogenesis. *N. Engl. J. Med.* **358**, 2039-2049.

Kimura, H., Miyashita, H., Suzuki, Y., Kobayashi, M., Watanabe, K., Sonoda, H., Ohta, H., Fujiwara, T., Shimosegawa, T. and Sato, Y. (2009). Distinctive localization and opposed roles of vasohibin-1 and vasohibin-2 in the regulation of angiogenesis. *Blood* **113**, 4810-4818.

Kobayashi, M., Nishita, M., Mishima, T., Ohashi, K. and Mizuno, K. (2006). MAPKAPK-2-mediated LIM-kinase activation is critical for VEGF-induced actin remodeling and cell migration. *EMBO J.* **25**, 713-726.

Leslie, J. D., Ariza-McNaughton, L., Bermange, A. L., McAdow, R., Johnson, S. L. and Lewis, J. (2007). Endothelial signalling by the Notch ligand Delta-like 4 restricts angiogenesis. *Development* **134**, 839-844.

Martin-Belmonte, F., Arvan, P. and Alonso, M. A. (2001). MAL mediates apical transport of secretory proteins in polarized epithelial Madin-Darby canine kidney cells. *J. Biol. Chem.* **276**, 49337-49342.

Muchowski, P. J., Schaffar, G., Sittler, A., Wanker, E. E., Hayer-Hartl, M. K. and Hartl, F. U. (2000). Hsp70 and hsp40 chaperones can inhibit self-assembly of polyglutamine proteins into amyloid-like fibrils. *Proc. Natl. Acad. Sci. USA* **97**, 7841-7846.

Nasu, T., Maeshima, Y., Kinomura, M., Hirokoshi-Kawahara, K., Tanabe, K., Sugiyama, H., Sonoda, H., Sato, Y. and Makino, H. (2009). Vasohibin-1, a negative feedback regulator of angiogenesis, ameliorates renal alterations in a mouse model of diabetic nephropathy. *Diabetes* **58**, 2365-2375.

Nickel, W. (2005). Unconventional secretory routes: direct protein export across the plasma membrane of mammalian cells. *Traffic* **6**, 607-614.

Nickel, W. (2007). Unconventional secretion: an extracellular trap for export of fibroblast growth factor 2. *J. Cell Sci.* **120**, 2295-2299.

Nickel, W. and Rabouille, C. (2009). Mechanisms of regulated unconventional protein secretion. *Nat. Rev. Mol. Cell Biol.* **10**, 148-155.

Ohta, H., Tsuji, T., Asai, S., Sasakura, K., Teraoka, H., Kitamura, K. and Kangawa, K. (1999). One-step direct assay for mature-type adrenomedullin with monoclonal antibodies. *Clin. Chem.* **45**, 244-251.

Petrucelli, L., Dickson, D., Kehoe, K., Taylor, J., Snyder, H., Grover, A., De Lucia, M., McGowan, E., Lewis, J., Prihar, G. et al. (2004). CHIP and Hsp70 regulate tau ubiquitination, degradation and aggregation. *Hum. Mol. Genet.* **13**, 703-714.

Piotrowicz, R. S., Martin, J. L., Dillman, W. H. and Levin, E. G. (1997). The 27-kDa heat shock protein facilitates basic fibroblast growth factor release from endothelial cells. *J. Biol. Chem.* **272**, 7042-7047.

Sabath, E., Negoro, H., Beaudry, S., Paniagua, M., Angelow, S., Shah, J., Grammatikakis, N., Yu, A. S. and Denker, B. M. (2008). Galpha12 regulates protein interactions within the MDCK cell tight junction and inhibits tight-junction assembly. *J. Cell Sci.* **121**, 814-824.

Sato, H., Abe, T., Wakusawa, R., Asai, N., Kunikata, H., Ohta, H., Sonoda, H., Sato, Y. and Nishida, K. (2009). Vitreous levels of vasohibin-1 and vascular endothelial growth factor in patients with proliferative diabetic retinopathy. *Diabetologia* **52**, 359-361.

Sato, Y. (2006). Update on endogenous inhibitors of angiogenesis. *Endothelium* **13**, 147-155.

Sato, Y. and Sonoda, H. (2007). The vasohibin family: a negative regulatory system of angiogenesis genetically programmed in endothelial cells. *Arterioscler. Thromb. Vasc. Biol.* **27**, 37-41.

Seelenmeyer, C., Wegehingel, S., Lechner, J. and Nickel, W. (2003). The cancer antigen CA125 represents a novel counter receptor for galectin-1. *J. Cell Sci.* **116**, 1305-1318.

Shen, J., Yang, X., Xiao, W. H., Hackett, S. F., Sato, Y. and Campochiaro, P. A. (2006). Vasohibin is up-regulated by VEGF in the retina and suppresses VEGF receptor 2 and retinal neovascularization. *FASEB J.* **20**, 723-725.

Shibuya, T., Watanabe, K., Yamashita, H., Shimizu, K., Miyashita, H., Abe, M., Moriya, T., Ohta, H., Sonoda, H., Shimosegawa, T. et al. (2006). Isolation and characterization of vasohibin-2 as a homologue of VEGF-inducible endothelium-derived angiogenesis inhibitor vasohibin. *Arterioscler. Thromb. Vasc. Biol.* **26**, 1051-1057.

Shimizu, K., Watanabe, K., Yamashita, H., Abe, M., Yoshimatsu, H., Ohta, H., Sonoda, H. and Sato, Y. (2005). Gene regulation of a novel angiogenesis inhibitor, vasohibin, in endothelial cells. *Biochem. Biophys. Res. Commun.* **327**, 700-706.

Siekmann, A. F. and Lawson, N. D. (2007). Notch signalling limits angiogenic cell behaviour in developing zebrafish arteries. *Nature* **445**, 781-784.

Sonoda, H., Ohta, H., Watanabe, K., Yamashita, H., Kimura, H. and Sato, Y. (2006). Multiple processing forms and their biological activities of a novel angiogenesis inhibitor vasohibin. *Biochem. Biophys. Res. Commun.* **342**, 640-646.

Takahashi, T., Tada, M., Igarashi, S., Koyama, A., Date, H., Yokoseki, A., Shiga, A., Yoshida, Y., Tsuji, S., Nishizawa, M. et al. (2007). Aprataxin, causative gene product for EAOH/AOA1, repairs DNA single-strand breaks with damaged 3′-phosphate and 3′-phosphoglycolate ends. *Nucleic Acids Res.* **35**, 3797-3809.

Tamaki, K., Moriya, T., Sato, Y., Ishida, T., Maruo, Y., Yoshinaga, K., Ohuchi, N. and Sasano, H. (2009). Vasohibin-1 in human breast carcinoma: a potential negative feedback regulator of angiogenesis. *Cancer Sci.* **100**, 88-94.

Torrado, L. C., Temmerman, K., Muller, H. M., Mayer, M. P., Seelenmeyer, C., Backhaus, R. and Nickel, W. (2009). An intrinsic quality-control mechanism ensures unconventional secretion of fibroblast growth factor 2 in a folded conformation. *J. Cell Sci.* **122**, 3322-3329.

Wakusawa, R., Abe, T., Sato, H., Yoshida, M., Kunikata, H., Sato, Y. and Nishida, K. (2008). Expression of vasohibin, an antiangiogenic factor, in human choroidal neovascular membranes. *Am. J. Ophthalmol.* **146**, 235-243.

Watanabe, K., Hasegawa, Y., Yamashita, H., Shimizu, K., Ding, Y., Abe, M., Ohta, H., Imagawa, K., Hojo, K., Maki, H. et al. (2004). Vasohibin as an endothelium-derived negative feedback regulator of angiogenesis. *J. Clin. Invest.* **114**, 898-907.

Wickner, S., Maurizi, M. R. and Gottesman, S. (1999). Posttranslational quality control: folding, refolding, and degrading proteins. *Science* **286**, 1888-1893.

Yamashita, H., Abe, M., Watanabe, K., Shimizu, K., Moriya, T., Sato, A., Satomi, S., Ohta, H., Sonoda, H. and Sato, Y. (2006). Vasohibin prevents arterial neointimal formation through angiogenesis inhibition. *Biochem. Biophys. Res. Commun.* **345**, 919-925.

Yamazaki, T., Yoshimatsu, Y., Morishita, Y., Miyazono, K. and Watabe, T. (2009). COUP-TFII regulates the functions of Prox1 in lymphatic endothelial cells through direct interaction. *Genes Cells* **14**, 425-434.

Yoshinaga, K., Ito, K., Moriya, T., Nagase, S., Takano, T., Niikura, H., Yaegashi, N. and Sato, Y. (2008). Expression of vasohibin as a novel endothelium-derived angiogenesis inhibitor in endometrial cancer. *Cancer Sci.* **99**, 914-919.

Genes to Cells

Up-regulation of *PSF1* promotes the growth of breast cancer cells

Izumi Nakahara[1,2], Mamiko Miyamoto[1], Tatsuhiro Shibata[3,4], Sadako Akashi-Tanaka[5], Takayuki Kinoshita[5], Kaoru Mogushi[2], Kohtaro Oda[1,2], Masaya Ueno[6], Nobuyuki Takakura[6], Hiroshi Mizushima[2], Hiroshi Tanaka[2] and Tsutomu Ohta[1]*

[1]*Center for Medical Genomics, National Cancer Center Research Institute, 5-1-1 Tsukiji, Chuo-ku, Tokyo 104-0045, Japan*
[2]*Department of Computational Biology, Tokyo Medical and Dental University, 1-5-45 Yushima, Bunkyo-ku, Tokyo 113-8510, Japan*
[3]*Pathology Division, National Cancer Center Research Institute, 5-1-1 Tsukiji, Chuo-ku, Tokyo 104-0045, Japan*
[4]*Cancer Genomics Project, National Cancer Center Research Institute, 5-1-1 Tsukiji, Chuo-ku, Tokyo 104-0045, Japan*
[5]*Breast Surgery Division, National Cancer Center Hospital, 5-1-1 Tsukiji, Chuo-ku, Tokyo 104-0045, Japan*
[6]*Department of Signal Transduction, Research Institute for Microbial Diseases, Osaka University, 3-1 Yamada-oka Suita, Osaka 565-0871, Japan*

PSF1 is a subunit of the GINS complex that functions along with the MCM2-7 complex and Cdc45 in eukaryotic DNA replication. Although mammalian *PSF1* is predominantly expressed in highly proliferating cells and organs, little is known about the roles of *PSF1* in mature cells or cancer cells. We found that PSF1 was expressed at relatively high levels in breast tumor cells, but at low levels in normal breast cells. Knockdown of *PSF1* expression using small interfering RNA (siRNA) slowed the growth of breast cancer cell lines by delaying DNA replication but did not affect proliferation of normal human mammary epithelial cells. Reduced *PSF1* expression also inhibited anchorage-independent growth in breast cancer cell lines. These results suggest that *PSF1* over-expression is specifically involved in breast cancer cell growth. Therefore, PSF1 inhibition might provide new therapeutic approaches for breast cancer.

Introduction

Chromosomal DNA replication is tightly regulated in eukaryotic cells. Origin-recognition complexes (ORC) are believed to play a central role in the recognition of replication origins (Labib & Gambus 2007). In the late M and early G1 phases of the cell cycle, the mini-chromosome maintenance 2-7 (MCM2-7) complex and Cdc45 are localized to DNA replication origins along with ORC (Labib & Gambus 2007). The MCM2-7 complex and Cdc45 unwind the parental DNA duplex, allowing DNA polymerases to initiate DNA synthesis (Labib & Gambus 2007). The GINS complex was recently reported to participate in both the initiation and elongation phases of DNA replication through its ability to recruit Cdc45 and DNA polymerase (Pai *et al.* 2009). The GINS complex, which contains PSF1, PSF2, PSF3 and SLD5, was first identified as a component of prerecognition complexes by genetic analyses in *Saccharomyces cerevisiae* (Takayama *et al.* 2003). Genes encoding the GINS components are evolutionally conserved (Kubota *et al.* 2003). *PSF1* gene expression is essential for early embryogenesis, maintenance of immature hematopoietic cell pool size and acute bone marrow regeneration in mice (Ueno *et al.* 2005, 2009). PSF1 is predominantly expressed in highly proliferating cells but not in mature cells (Ueno *et al.* 2005) and is up-regulated in intrahepatic cholangiocarcinomas (Obama *et al.* 2005). Recently, it was shown that up-regulated PSF1 expression drove tumorigenesis and conferred metastatic properties (Nagahama *et al.* 2010). However, the role of *PSF1* in normal mature cells or mammalian cancer cells remains unclear.

In this study, we show that *PSF1* expression is up-regulated in breast cancer tissues and cell lines. Down-regulation of *PSF1* expression led to reduced growth of cancer cells, but not of normal mammary epithelial cells. Reduced *PSF1* expression also inhibited the anchorage-independent cell growth of breast

Communicated by: Masayuki Yamamoto (Tohoku University)
**Correspondence*: cota@ncc.go.jp

DOI: 10.1111/j.1365-2443.2010.01442.x

cancer cell lines. These findings indicate that PSF1 might have potential as a breast cancer biomarker and as a gene target for breast cancer treatment.

Results

PSF1 protein expression is enhanced in breast cancer cells

As *PSF1* promoter activity can be stimulated *in vitro* via 17β-estradiol (E2)-mediated estrogen receptor (ER) signaling (Hayashi *et al.* 2006), we speculated that *PSF1* expression might be up-regulated in breast cancer cells. To examine PSF1 expression in breast cancer tissues, we performed an immunostaining analysis of 34 tissue specimens. PSF1 immunohistochemical staining in normal breast tissues was very weak but was significantly enhanced in 41% (14 of 34) of cancer tissue specimens (Fig. 1A and Table 1). We also found that PSF1 was highly expressed in the invasive tumor area (Fig. 1B), suggesting that PSF1 might be predominantly expressed in advanced malignancy cells. The relationship between the level of PSF1 expression and clinicopathological parameters was also investigated, although no significant associations between the level of PSF1 expression and prognostic indicators could be established in the breast cancer specimens tested (Table 1). Next, to examine whether PSF1 expression correlated with hormone receptor expression and breast cancer biomarkers, we analyzed the expression of ER, progesterone receptor (PgR), human epidermal growth factor receptor type 2 (HER2) and tumor suppressor gene product p53 by immunohistochemical staining of the same breast cancer samples used previously. No correlation between the expression of PSF1 and that of hormone receptors or breast cancer biomarkers was observed (Table 1), suggesting that PSF1 protein expression is not affected by hormone receptors (ER and PgR) or breast cancer biomarkers (HER2 and p53).

We analyzed the association between PSF1 expression and prognosis. The observation time (range: 0.6–3.4 years, median: 3.2 years) after surgery for the 34 patients did not allow for analysis of either the 5-year survival rate or 3-year disease-free survival rate. Therefore, we investigated *PSF1* expression levels and analyzed the survival rate using a publicly available microarray dataset of 295 patients with breast cancer (http://microarray-pubs.stanford.edu/wound_NKI/explore.html). Figure 1C shows the survival rates of the 127 and 168 patients who respectively had high and low *PSF1* expression levels. The 15-year survival rate of the low *PSF1* expression level group was higher ($P = 0.00466$), suggesting that *PSF1* expression might be a prognostic marker.

Promoter activity of *PSF1* is up-regulated in breast cancer cells

To examine *PSF1* expression in cell lines, we analyzed *PSF1* mRNA expression levels in breast cancer cell lines and normal breast cells using real-time RT-PCR. High *PSF1* expression levels were observed in breast cancer cell lines (Fig. 2A, lanes 3–5; upper panel), whereas only low levels were detected in normal human mammary epithelial cells (HMEC) or immortalized HMEC by expression of hTERT (catalytic component of human telomerase) (HMEC-tert) (Fig. 2A, lanes 1 and 2; upper panel). Next, we analyzed PSF1 protein levels in breast cancer cell lines and normal breast cells by Western blotting using anti-PSF1 antibody. PSF1 proteins were detected at high levels in breast cancer cell lines, but at low levels in HMEC and HMEC-tert cells (Fig. 2A; lower panel). These results suggested that both *PSF1* mRNA and PSF1 protein expressions were enhanced in breast cancer cell lines. We also analyzed the expression levels of the other GINS complex subunits (*PSF2, PSF3* and *SLD5*) in normal breast cells and breast cancer cell lines. Like *PSF1* expression, *SLD5* expression was up-regulated in all three breast cancer cell lines tested (Fig. 2B; lower panel), whereas expression levels of *PSF2* and *PSF3* were only up-regulated in specific breast cancer cell lines (Fig. 2B; upper and middle panels).

Because gene amplification of cancer-related genes has been observed in cancer cells, we investigated the possibility of *PSF1* gene amplification using a single-nucleotide polymorphism (SNP) chip. SNP IDs were rs2500406 and rs6083862. No amplification of the *PSF1* gene locus was detected in any of the breast cancer cell lines tested (data not shown), which suggested that *PSF1* up-regulation in breast cancer cell lines was not because of *PSF1* gene amplification. We then analyzed *PSF1* promoter activity using different promoter region lengths: 5, 1.6 and 0.5 kb upstream from the transcriptional start site. We found that when of each of the three regions was fused to the luciferase gene in T47D cells, the promoter activities were more than 10 times higher than those observed in HMEC-tert (Fig. 3A). This result indicated that the up-regulated *PSF1* expression was because of increased promoter activity of *PSF1* in breast cancer cells.

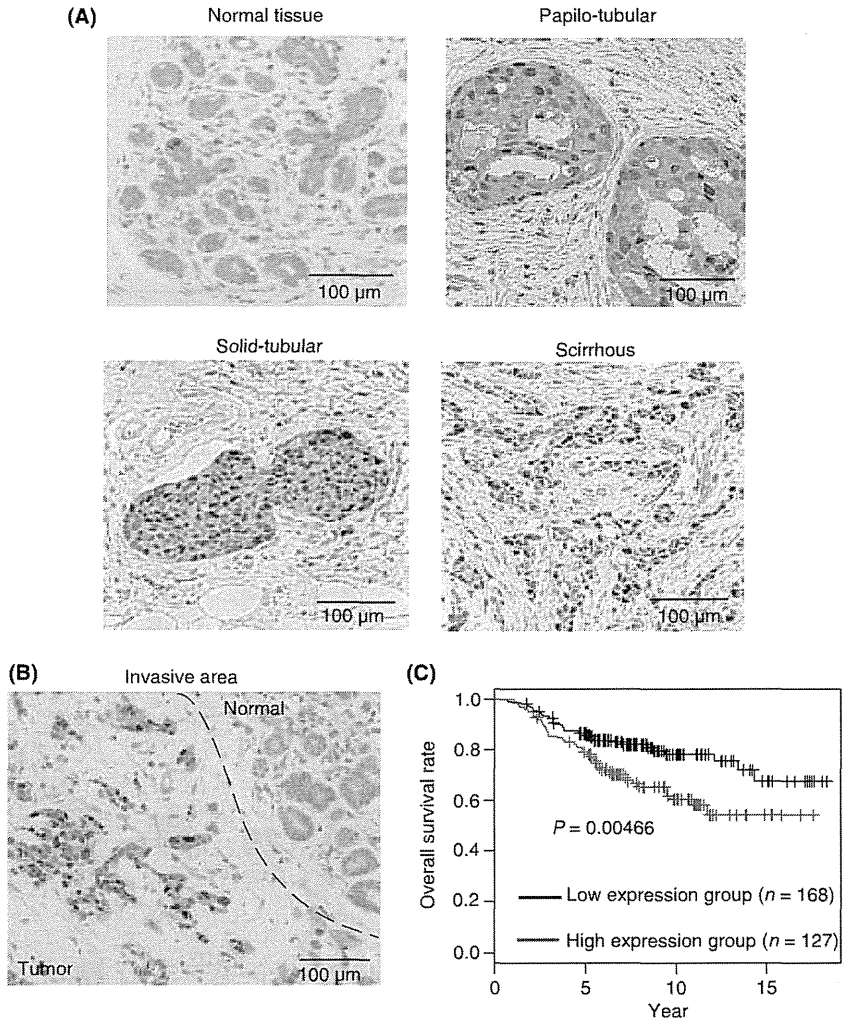

Figure 1 Increased PSF1 expression in human breast cancer tissues. Immunohistochemical staining of PSF1 in human breast cancer samples using anti-PSF1 antibody. Bars indicate 100 μm. (A) Nuclear PSF1 expression was detected in three types of breast cancer (papillo-tubular, solid-tubular and scirrhous). In rare cases, nuclear PSF1 was also detected in a few normal mammary epithelial cells located in the lobule where cell proliferation occurs physiologically. (B) Prominent and frequent nuclear accumulation of PSF1 was detected in invasive carcinoma cells (in tumor area), whereas no positive staining was observed in noncancerous mammary duct epithelium (in normal area). (C) The relationship between the level of *PSF1* expression and the survival rate in patients with breast cancer. The relationship between *PSF1* expression levels and the survival rate was analyzed by using publicly available microarray dataset of 295 patients with breast cancer (http://microarray-pubs.stanford.edu/wound_NKI/explore.html). The survival rates were determined using the Kaplan–Meier methods and were compared by means of the log rank test. The gray line shows a survival curve for 127 patients with higher *PSF1* expression levels and the black line for 168 patients with lower *PSF1* expression levels. The cutoff value of *PSF1* expression level was calculated by taking the mean value of the median expression levels of the good prognosis group (over 5-year survival) and the poor prognosis group (<5-year survival), respectively.

Down-regulation of *PSF1* led to reduced growth of breast cancer cells

To determine whether knockdown of *PSF1* expression impacted the growth of breast cancer cells, we measured the growth rate of breast cancer cell lines and normal cells treated with *PSF1*-specific siRNA. Knockdown of *PSF1* expression was detected by real-time RT-PCR in breast cancer cells (T47D, MDA-MB-231 and MDA-MB-361) and normal human mammary epithelial cells (HMEC and HMEC-tert) (Fig. 3B and Fig. S1 in Supporting

Table 1 Clinicopathologic features and immunohistochemical results of PSF1, ER, PgR, HER2 and p53

Patient number	PSF1	ER	PgR	HER2	p53	Stage	Histology
BC-1	0.5	0	0	3	2	2B	Papillo-tubular
BC-2	0.5	1	3	1	0	2A	Scirrhous
BC-3	1	2	3	2	0	1	Solid-tubular
BC-4	0.5	2	3	1	1	2A	Scirrhous
BC-5	1	2	3	0	1	2A	Scirrhous
BC-6	1	3	2	1	1	3B	Papillo-tubular
BC-7	2	1	1	0	2	1	Scirrhous
BC-8	2	3	3	1	0	1	Papillo-tubular
BC-9	2	3	1	1	2	2B	Scirrhous
BC-10	2	0	1	1	0	1	Papillo-tubular
BC-11	2	0	1	3	1	3A	Solid-tubular
BC-12	1	3	3	3	2	2B	Solid-tubular
BC-13	2	3	0	1	1	2A	Papillo-tubular
BC-14	2	1	2	3	2	3A	Solid-tubular
BC-15	1	0	0	1	2	1	Solid-tubular
BC-16	0.5	1	3	1	2	1	Scirrhous
BC-18	0.5	0	1	0	2	2B	Solid-tubular
BC-19	2	0	0	0	1	2A	Solid-tubular
BC-20	0.5	2	2	0	0	2A	Solid-tubular
BC-21	2	0	0	0	2	2A	Scirrhous
BC-22	0.5	1	3	0	0	2B	Solid-tubular
BC-23	2	0	3	1	2	2A	Scirrhous
BC-24	0.5	0	1	1	1	2A	Papillo-tubular
BC-25	1	2	2	0	2	2A	Solid-tubular
BC-26	0.5	1	2	0	0	1	Papillo-tubular
BC-28	2	3	3	0	1	1	Solid-tubular
BC-29	2	0	3	1	0	2A	Solid-tubular
BC-30	0.5	0	0	0	0	1	Scirrhous
BC-31	2	0	0	0	2	2A	Solid-tubular
BC-32	0.5	3	3	0	1	1	Papillo-tubular
BC-34	1	0	0	3	1	1	Papillo-tubular
BC-35	0.5	2	2	0	2	2B	Scirrhous
BC-36	0.5	2	3	0	1	2A	Papillo-tubular
BC-37	2	0	0	0	0	1	Solid-tubular

Staining extent was scored on a scale of 0–2 for PSF1, as follows: 0 = no staining, 0.5 = <5%, 1 = 5%–30% and 2 = >30% of tumor cells. Tumor cells with staining intensity 2 were considered as positive. Staining extent was scored on a scale of 0–3 for ER and PgR, as follows: 0 = no staining, 1 = <10%, 2 = 1%–10% and 3 = >10% of tumor cells. Tumor cells with staining intensity 3 were considered as positive. Staining extent was scored on a scale of 0–3 for HER2, as follows: 0 = no staining, 1 = <10%, 2 = 10%–30% and 3 = >30% of tumor cells. Tumor cells with staining intensity 2 and 3 were considered as positive. Staining extent was scored on a scale of 0–2 for p53, as follows: 0 = no staining, 1 = weak staining and 2 = strong staining in tumor cells. Tumor cells with staining intensity 2 were considered as positive.
ER, estrogen receptor; Pgr, progesterone receptor.

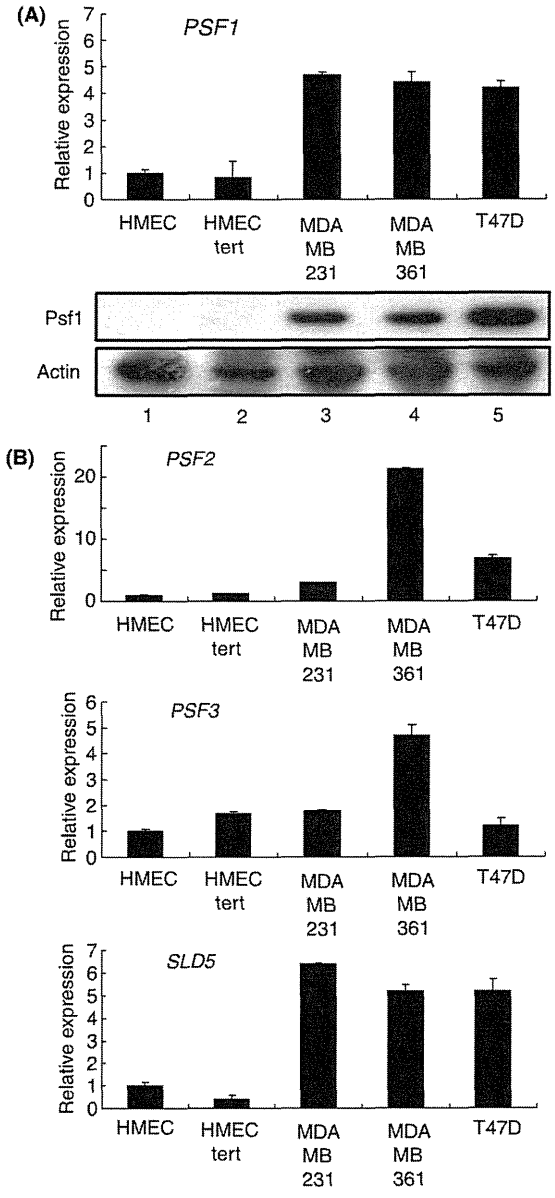

Figure 2 Expression levels of subunits of GINS in cell lines. (A) *PSF1* expression levels in cell lines. *PSF1* expressions in normal human mammary epithelial cells, HMEC and HMEC-tert (lanes 1 and 2) and in breast cancer cell lines, MDA-MB-231, MDA-MB-361 and T47D (lanes 3-5) were analyzed by real-time RT-PCR (upper panel) and by immunoblotting (lower panel). Level of *PSF1* expression in HMEC cells was set at 1. *CTBP1* and actin were internal controls. Data show the mean ± SEM (n = 3). (B) Expressions of *PSF2*, *PSF3* and *SLD5* in normal human mammary epithelial cells (HMEC and HMEC-tert) and in breast cancer cell lines (MDA-MB-231, MDA-MB-361 and T47D cells) were analyzed by real-time RT-PCR. Level of each gene expression in HMEC cells was set at 1. *CTBP1* was internal control. Data show the mean ± SEM (n = 3).

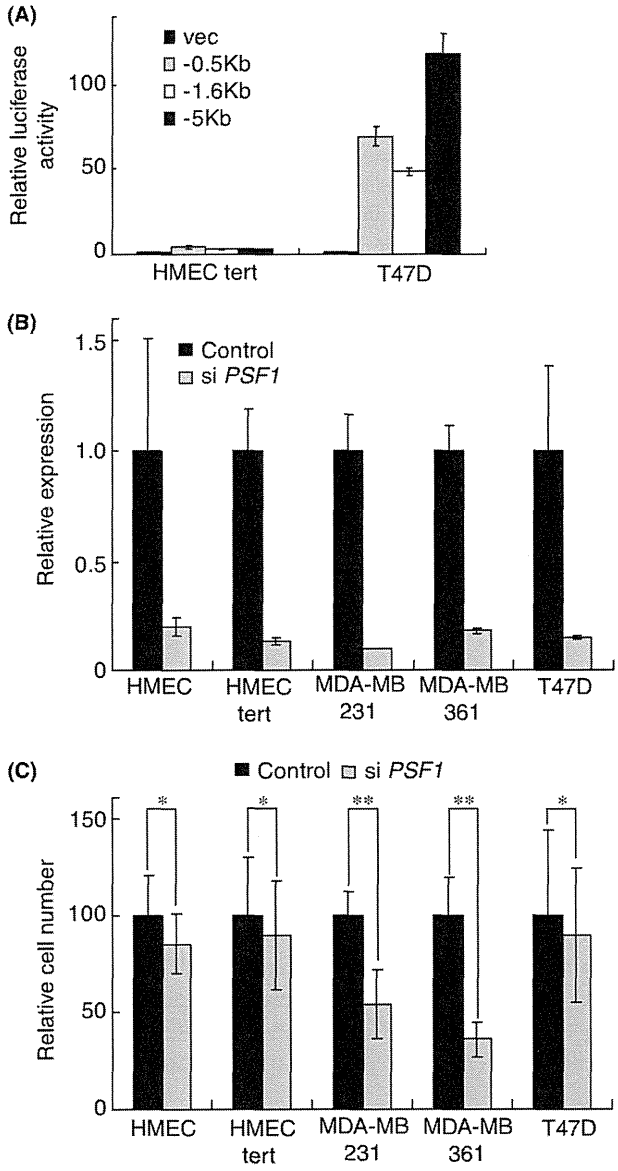

Figure 3 Up-regulation of *PSF1* promotes growth of breast cancer cell lines. (A) *PSF1* promoter (−0.5, −1.6 and −5 kb) activity using luciferase assay in normal human mammary epithelial cells (HMEC) and breast cancer cells. The pGL3-basic reporter plasmid (vec) containing the *PSF1* promoter (100 ng) was transfected into HMEC-tert and T47D cells. Luciferase activity in cell lysates was normalized to the *Renilla* luciferase activity of p RL-TK as an internal control. The activity in the absence of *PSF1* promoter was set at 1. Data show the mean ± SEM (n = 3). (B) Knockdown of *PSF1* expression by *PSF1* siRNA. The control siRNA or *PSF1* siRNA was transfected into HMEC, HMEC-tert, MDA-MB-231, MDA-MB-361 and T47D cells. After 2 days, the expression level of *PSF1* in the cells was analyzed by real-time RT-PCR. Level of *PSF1* expression in cells transfected with control siRNA was set at 1. *GAPDH* was an internal control. Data show the mean ± SEM (n = 3). (C) Growth rate of breast cancer cells by knockdown of *PSF1*. Six days after transfection of siRNA, cell numbers were counted. The number of cells transfected with control siRNA was set at 100. Data show the mean ± SEM, $*P > 0.05$, $**P < 0.01$ (n = 3).

Information). Six days after transfection, the numbers of HMEC, HMEC-tert and T47D cells transfected with either *PSF1*-specific or control siRNA were similar (Fig. 3C and Fig. S2 in Supporting Information). In contrast, MDA-MB-231 and MDA-MB-361 cell numbers after transfection with *PSF1*-specific siRNA were approximately 50% and 40%, respectively, of those transfected with control siRNA (Fig. 3C and Fig. S2 in Supporting Information). These results indicated that *PSF1* over-expression promoted growth in MDA-MB-231 and MDA-MB-361 cells, but not in normal HMEC and T47D cells.

To examine whether other components of the GINS complex were necessary for the growth of normal HMEC and breast cancer cells, we analyzed cell growth after knockdown of *PSF2*, *PSF3* and *SLD5* expression. Knockdown of these genes was confirmed by real-time RT-PCR (Fig. S3 in Supporting Information). Growth of normal human mammary epithelial cells (HMEC-tert) after knockdown of these three genes was not significantly influenced (Fig. 4A). In contrast, growth of breast cancer cells (MDA-MB-231) was reduced by knockdown of *PSF2* and *SLD5*, similar to that of *PSF1* (Fig. 4A; upper and lower panels) and was weakly reduced by knockdown of *PSF3* (Fig. 4A; middle panel). As the amount of PSF1 might be regulated by PSF2, PSF3 and SLD5, we analyzed the levels of *PSF1* mRNA and PSF1 protein after knockdown of GINS complex subunit expression. Reduced expression of *PSF2*, *PSF3* or *SLD5* had no effect on the level of *PSF1* mRNA (Fig. 4B; upper panel), but the level of PSF1 protein decreased (Fig. 4B; lower panel). This result could indicate that PSF1 protein is stabilized in the GINS complex in breast cancer cells.

Slow cell growth in response to reduced PSF1 expression due to delayed DNA replication

To examine whether *PSF1* knockdown induced apoptosis in breast cancer cells, we analyzed cell apoptosis using a fluorochrome inhibitor that covalently

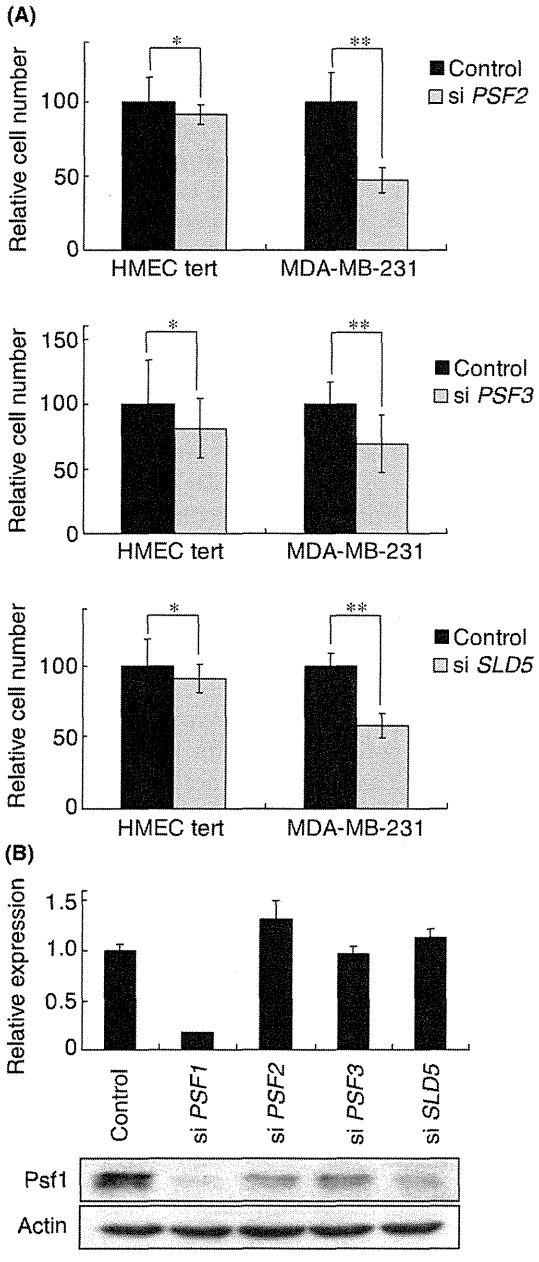

Figure 4 Knockdown of GINS complex subunits reduces growth of breast cancer cells. (A) Growth rate of normal cells and breast cancer cells by knockdown of *PSF2* (upper), *PSF3* (middle) and *SLD5* (lower). Control, *PSF2*, *PSF3* or *SLD5* siRNA was transfected into HMEC-tert or MDA-MB-231 cells. Six days after transfection of siRNA, cell numbers were counted. The number of cells transfected with control siRNA was set at 100. Data show the mean ± SEM, $*P > 0.05$, $**P < 0.01$ ($n = 3$). (B) Expression levels of *PSF1* mRNA and PSF1 protein in MDA-MB-231 cells transfected with siRNA of GINS complex subunits. Control, *PSF1*, *PSF2*, *PSF3* or *SLD5* siRNA was transfected into MDA-MB-231 cells. After 2 days, the expression level of *PSF1* was analyzed by real-time RT-PCR (upper panel). Level of *PSF1* expression in cells transfected with control siRNA was set at 1. *GAPDH* was an internal control. Data show the mean ± SEM ($n = 3$). Four days after transfection of siRNA, cells were collected and lysed by RIPA buffer. PSF1 protein was detected by anti-PSF1 antibody (lower panel). Actin was an internal control. HMEC, human mammary epithelial cells.

binds to active caspases (Bedner *et al.* 2000; Ishida *et al.* 2007). At 3 or 6 days after transfection with either control or *PSF1* siRNA, caspase-positive cells were not detected in the ~400 MDA-MB-231 cells examined (data not shown). Next, to determine whether *PSF1* knockdown affected the cell cycle, we analyzed DNA content using flow cytometry 5 days after transfection of breast cancer cells or normal cells with *PSF1* siRNA. FACS analysis showed that the number of cells in the cell cycle S phase increased after *PSF1* knockdown in MDA-MB-231 and MDA-MB-361 cells, but not in HMEC-tert cells (Fig. 5A). This result indicated that *PSF1* might participate in the S phase of the cell cycle in breast cancer cells, but not in normal HMEC. EdU incorporation assays were then performed in cells treated with *PSF1* siRNA. At 72 h after *PSF1* knockdown, EdU was incorporated for 75 min in cells. *PSF1* knockdown reduced cellular EdU incorporation in breast cancer cell lines (MDA-MB-231 and MDA-MB-361), but not normal human mammary epithelial cells (HMEC-tert) (Fig. 5B and C). These results supported the finding that reduction of *PSF1* levels slowed cell growth by delaying DNA replication in breast cancer cell lines.

Down-regulation of *PSF1* repressed anchorage-independent growth of breast cancer cells

To determine whether *PSF1* expression knockdown affected anchorage-independent breast cancer cell growth, we analyzed colony-formation activity of MDA-MB-231, MDA-MB-361 and T47D cells treated with *PSF1* siRNA on soft agar. Although MDA-MB-361 cells did not form colonies on soft agar (data not shown), 3 weeks after treatment, the number of colonies formed from T47D and MDA-MB-231 cells transfected with *PSF1*-specific siRNA was reduced approximately 40% and 10%, respectively, compared to those from cells transfected with control siRNA (Fig. 6). This result suggested that up-regulation of *PSF1* induced anchorage-independent growth of breast cancer cells.